



**University of Minho**  
*Engineering School*  
*Civil Engineering Department*

## **Seismic strengthening of beam-column joints with multi-directional CFRP laminates**

Mário Coelho, Pedro Fernandes, José Sena Cruz, Joaquim Barros

Technical Report 11-DEC/E-13

Technical report developed under the scope of project  
*PTDC/ECM/74337/2006.*

**Date:** April 2011  
**Nº of pages:** 47

**Keywords:** MDL-CFRP; MF-EBR; RC joint; plain rebar; seismic retrofit



## GENERAL INDEX

<b>1</b>	<b>INTRODUCTION .....</b>	<b>7</b>
<b>2</b>	<b>EXPERIMENTAL PROGRAM.....</b>	<b>10</b>
2.1	TEST SPECIMENS.....	10
2.2	MATERIAL CHARACTERIZATION.....	18
2.3	SPECIMENS PREPARATION.....	20
<b>3</b>	<b>RESULTS.....</b>	<b>24</b>
3.1	DISPLACEMENT <i>VERSUS</i> FORCE.....	24
3.2	DISSIPATED ENERGY.....	28
3.3	STIFFNESS.....	30
3.4	STRAINS.....	30
3.5	FAILURE MODES.....	32
<b>4</b>	<b>CONCLUSIONS .....</b>	<b>32</b>
<b>5</b>	<b>ACKNOWLEDGMENTS.....</b>	<b>33</b>
<b>6</b>	<b>REFERENCES .....</b>	<b>34</b>



## FIGURES INDEX

Figure 1 – Type of joint studied.....	10
Figure 2 – Specimens (beam-column joints): a) global geometry; b) cross sections and reinforcing steel detail. ....	11
Figure 3 – Test setup: (a) General appearance of all the elements of the test setup; (b) Structural scheme obtained; (c) In situ photo.....	12
Figure 4 – Strengthening solution with MDL-CFRP. ....	16
Figure 5 – Location of the external instrumentation used for monitoring the tests. ....	17
Figure 6 – Location of the strain gauges. ....	18
Figure 7 – Joint rotation. ....	20
Figure 8 – Joint reconstruction: (a) formwork; (b) grout preparation; (c) filling the formwork with grout; (d) surface regularization.....	21
Figure 9 – Sealing the cracks: (a) formwork removal; (b) cracks sealing, with iron mass and purges application; (c) injection of the sealing resin; (d) final appearance of the joint after sealing the cracks.....	22
Figure 10 – MDL-CFRP application: (a) Creation of roughness on the concrete surface; (b) appearance of the treated area where the laminate would be glued. ....	23
Figure 11 – Displacement versus Force registered by load cell C1: (a) JD and JDR; (b) JD and JDR envelopes; (c) JPA-1 and JPA-1R; (d) JPA-1 and JPA-1R envelopes; (e) JPA-2 and JPA-2R; (f) JPA-2 and JPA-2R envelopes. ....	25
Figure 12 – Determination of the idealized elasto-perfectly plastic force versus displacement relationship (adapted from EN 1998-1:2004 (E)). ....	26
Figure 13 – Displacement ductility: (a) JD; (b) JDR; (c) JPA-1; (d) JPA-1R; (e) JPA-2; (f) JPA-2R. ....	27
Figure 14 – Dissipated energy: (a) JD/JDR; (b) JPA-1/JPA-1R/JPA-2R.....	29
Figure 15 - Stiffness degradation: (a) JD/JDR; (b) JPA-1/JPA-1R/JPA-2R.....	30
Figure 16 – Strain results (a) JDR specimen test; (b) JPA-1R specimen test; (c) JPA-2R specimen test. ....	31
Figure 17 – Damage in the joints after the tests: (a) JDR; (b) JPA-1R; (c) JPA-2R.....	32



## **TABLES INDEX**

Table 1 – Parameters for the tests in the first phase. ....	13
Table 2 – Strengthening solutions and test parameters for the second phase. ....	15
Table 3 – Mechanical properties of the rebars used in the joints.....	19
Table 4 – MDL-CFRP properties. ....	19
Table 5 – Maximum forces registered by load cell C1. ....	26
Table 6 – Displacement ductility of JD specimens. ....	28
Table 7 – Dissipated Energy of JD specimens.....	29



## NOMENCLATURE

$d_c$	Displacement at the top of the column
$d_u^-$	Ultimate displacement in the negative branch of the idealized elasto-perfectly plastic force <i>versus</i> displacement relationship
$d_u^+$	Ultimate displacement in the positive branch of the idealized elasto-perfectly plastic force <i>versus</i> displacement relationship
$d_y^-$	Yielding displacement in the negative branch of the idealized elasto-perfectly plastic force <i>versus</i> displacement relationship
$d_y^+$	Yielding displacement in the positive branch of the idealized elasto-perfectly plastic force <i>versus</i> displacement relationship
$F_c$	Horizontal force in the top of the column
$k_0$	Initial stiffness
$k_{s,0}$	Initial secant stiffness
$N_c$	Axial force in the column
$f_{ck}$	Concrete characteristic compressive strength
$f_{cm}$	Concrete average compressive strength
$E_s$	Steel Young modulus
$F_{s,um}$	Steel ultimate stress
$F_{s,ym}$	Steel yielding stress
$u$	Reduced axial force
B1	Inductive linear position sensor
C1	Hydraulic actuators equipped with a load cell of 200 kN capacity
C2	Hydraulic actuators equipped with a load cell of 500 kN capacity
C3	Load cell of 300 kN capacity
C4	Load cell of 100 kN capacity
LVDT	Linear variable differential transducers
P	Potentiometer
SG	Strain gauge



## GLOSSARY

EBR	Externally Bonded Reinforcement
FRP	Fibre Reinforced Polymers
MDL-CFRP	Multidirectional Laminate of Carbon Fibre Reinforced Polymer
MF-EBR	Mechanically Fastened and Externally Bonded Reinforcement
MF-FRP	Mechanically Fastened Fibre Reinforced Polymer
NSM	Near-Surface Mounted
RC	Reinforced Concrete



## 1 INTRODUCTION

### **Beam-Column Joints**

In the scope of the project on which this work was developed, is intended to apply multi-directional carbon fibre reinforced polymer laminates (MDL-CFRP) to strengthen reinforced concrete (RC) beam-column joints that have been subjected to seismic action. In this context, is important to know the characteristics of the type node of frame that needs seismic strengthening. In the next paragraphs a brief historical overview of the evolution of RC construction in Portugal is presented that will justify the type node of frame selected to be studied in this work.

Although there are some references to the existence of RC elements in building construction since the late nineteenth century, until the 1940s the construction of buildings with masonry structures and wooden floors continued to dominate, being only replaced by slabs with iron beams or RC in the kitchens, bathrooms and terraces (Lopes et al. 2008).

Only since the 1950s the construction of residential buildings began to replace the resistant masonry by reticulated frame structures constituted by RC beams and columns.

Until the end of the 1970s there were little specific regulations for such structures. Noteworthy was the publication in 1961 of RSEP (*Regulamento de Solicitações em Edifícios e Pontes*, in Portuguese) and REBA in 1967 (*Regulamento de Estruturas de Betão Armado*, in Portuguese). This fact, associated to the lack of supervision and/or application of the referred regulations lead to that, during this time, the buildings were constructed with no concern about the problems of durability of the concrete and with no solid theory bases of what would become the Earthquake Engineering (Lopes et al. 2008).

In this context, representative buildings of the end of the 1970s were selected for analysis in this study. With almost half a century, they have already reached the lifetime predicted by the current regulations for residential buildings and are most worthy of concern from the standpoint of strengthening and/or rehabilitation of them.

### **Strengthening Technique**

There are several reasons to need to strengthen existing RC structures. For example, natural disasters (earthquakes), material deterioration, changes in type of use (change of loading), problems in design (poor detail or configuration of the reinforcing steel, insufficient cross-section in columns), among others (Mukherjee e Joshi, 2005).



The main existent strengthening techniques to solve the problems mentioned above can be grouped as follows: repair with epoxy (injection of epoxy resin in the cracks of the elements lightly degraded), removal and replacement of concrete in more damaged areas, jacketing with RC layers, masonry blocks or steel plates, and also the use of composite materials (Engindeniz et al. 2004).

Among the different referred techniques, higher focus will be given to the strengthening with composite materials, namely, the use of *Fibre Reinforced Polymers* (FRPs). These can be applied by glue, on the surface of the structural elements to be strengthened, FRP fabrics or strips or through the insertion of FRP strips or rods in slits opened on the cover concrete. The techniques associated to those procedures are the *Externally Bonded Reinforcement* (EBR) and *Near-Surface Mounted* (NSM), respectively (ACI 2008).

The main advantages of such strengthening systems are the high strength/weight ratio, corrosion resistance, ease of application, low occupancy of useful interior space of buildings, low increase in the size of the elements after being reinforced, low labour costs and the great workability that is accomplished with such materials because they can be designed and adjusted as more convenient in every case (Bakis et al. 2002).

However, some disadvantages have been pointed out regarding to those two techniques, namely, the high initial cost of the reinforcing system, the fact that they do not allow the adequate exploitation of the tensile potentialities of FRP systems (the maximum stress installed in the FRP at failure of the strengthened element is much lower than its tensile strength) and the fragile rupture modes that occur before the formation of plastic hinges on the elements of the node (Bakis et al. 2002).

The typical failure modes in such cases are the FRP debonding when the EBR technique is used (CNR 2004) and, when NSM technique is applied, concrete cover rip-off (Barros and Fortes 2005).

In order to avoid premature failure of the FRP system, complements have been applied to the aforementioned strengthening techniques, such as the application of anchor systems composed of steel plates bolted in the ends of the FRP or the use of strapping with FRP fabric. In addition to the stress concentration that these localized interventions introduce in the elements to strengthen, they require differentiated and time consuming tasks that can compromise the competitiveness of these techniques.

In alternative to these techniques, a quite new technique, called *Mechanically Fastened Fibre Reinforced Polymers* (MF-FRP), has been proposed based on the use of steel fasteners applied along the laminate's length. The application of the MF-FRP





technique in the flexural strengthening of RC elements improves the flexural capacity with little or no loss in ductility (Bank 2004).

Nevertheless, some notable disadvantages of this system have been observed, including scale effects, cracking induced by the impact of fasteners in high-strength concrete and less-effective stress transfer between the FRP and concrete due to the discrete attachment points (Ray et al. 2000).

As previously mentioned, in this project context, the technique that is used in this study intends to change the rupture mode of the strengthening system to a more ductile one through the application of MDL-CFRP simultaneously glued and anchored to the surface of the strengthened elements. This technique designated *Mechanically Fastened and Externally Bonded Reinforcement* (MF-EBR) combines the fasteners from the MF-FRP technique with the externally glued properties from the EBR one.

In this context, three interior RC beam-column joints were reinforced according to the MF-EBR technique. This report presents the entire test program that was developed, including test configurations, results and corresponding analysis.

## 2 EXPERIMENTAL PROGRAM

The experimental program developed intends to study the behaviour under seismic action of beam-column joints representative of RC buildings existent in Portugal and built before the 1970s and the possibility of strengthening by the use of MF-EBR technique.

In this work, three interior joints like the one shown in Figure 1 were selected. Those were intended to simulate the connection of two beams with  $0.30 \times 0.40 \text{ m}^2$  cross section and 4 m span length and two columns with  $0.30 \times 0.30 \text{ m}^2$  cross section and 3 m length.

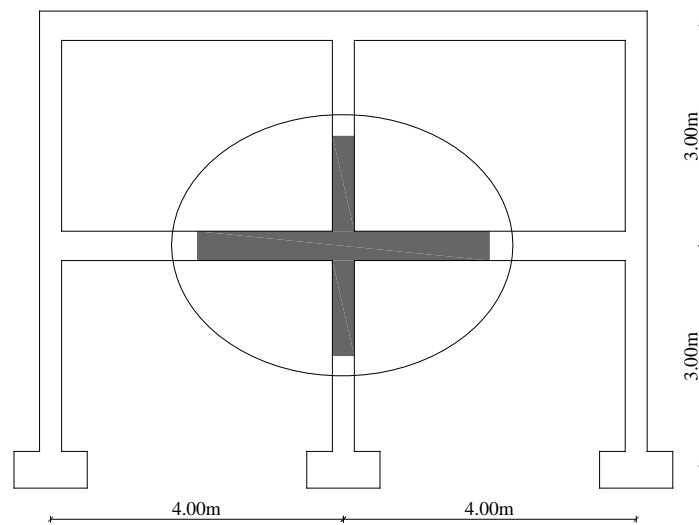


Figure 1 – Type of joint studied.

### 2.1 Test Specimens

Figure 2 presents the global geometry and the cross sections of the nodes. All the specimens have the same amount and detail of reinforcement steel. The anchorage of the longitudinal bars was carried out by a standard bend with a length of 0.10 m (Figure 2a). The beam longitudinal reinforcement was composed of 2 steel bars of 12 mm of diameter ( $2\text{Ø}12$ ) at the top and  $4\text{Ø}12$  at the bottom. The transverse reinforcement consisted in 8 mm stirrups spaced 0.20 m. In the columns, the longitudinal reinforcement was composed of 4 steel rebars of 12 mm diameter (one on each corner) and the transverse reinforcement was composed of 8 mm stirrups spaced 0.25 m between them. The anchorage of the transverse reinforcement was done like in the longitudinal reinforcement (see Figure 2b). The concrete cover was 2 cm thick for all the elements (beam and column).

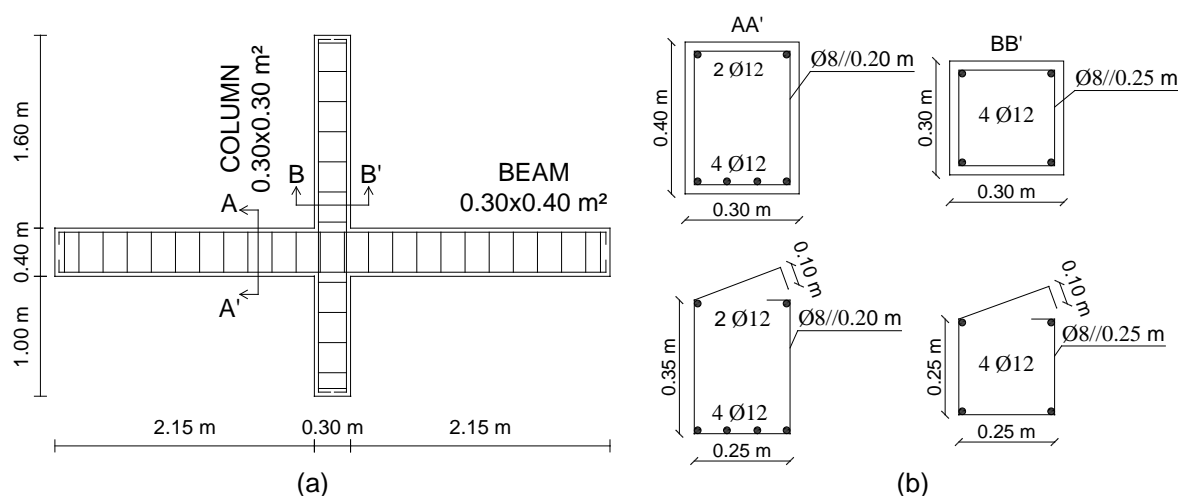


Figure 2 – Specimens (beam-column joints): a) global geometry; b) cross sections and reinforcing steel detail.

With this geometry configuration and the test setup used (see Figure 3a) the structural scheme of the joints was as presented in Figure 3b. In this figure, C1 and C2 represent the hydraulic actuators used to apply the lateral load at the top of the column and the axial force, respectively. C3 and C4 represent the load cells that were placed at the column support in order to register the reactions during the tests.  $N_c$  is the axial force induced in the column through C2,  $d_c$  and  $F_c$  are the displacement and the horizontal force on the top of the column.

The specimens were tested in the horizontal plane so, in order to minimize the internal forces and the vertical displacements associated to self-weight load, the specimens were supported vertically in four points. To minimize the friction between the support and the specimen during the lateral movement, a device composed by spheres with reduced friction was adopted. These were located at the centre of the squares that can be seen in Figure 3a under the specimen.

The horizontal displacements were allowed in the longitudinal direction of the beams through a bearing system used at their ends that only restricts the transverse displacement of them.

The total friction forces achieved with the spheres and bearing systems were found to be negligible (Fernandes et al. 2011).

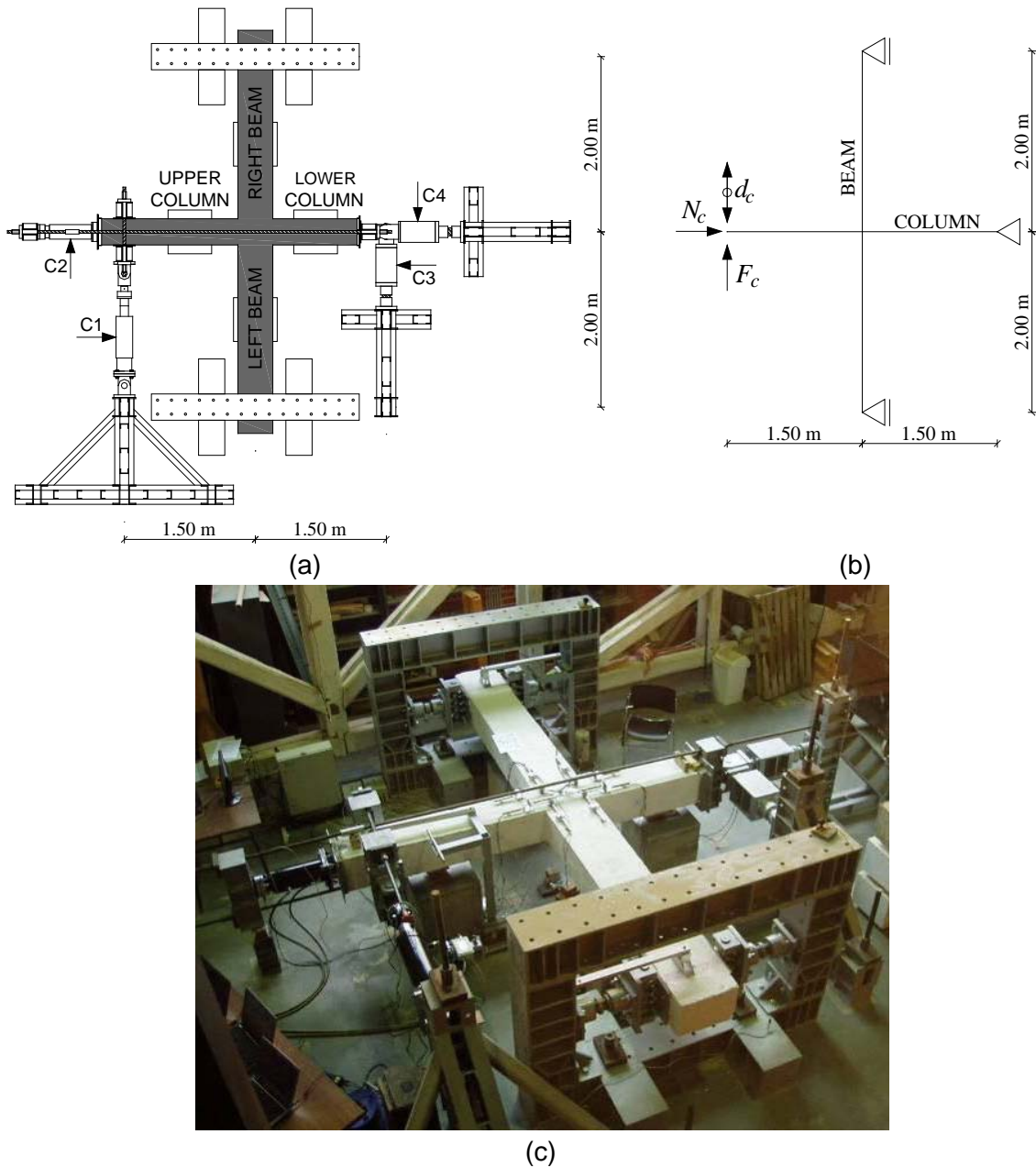
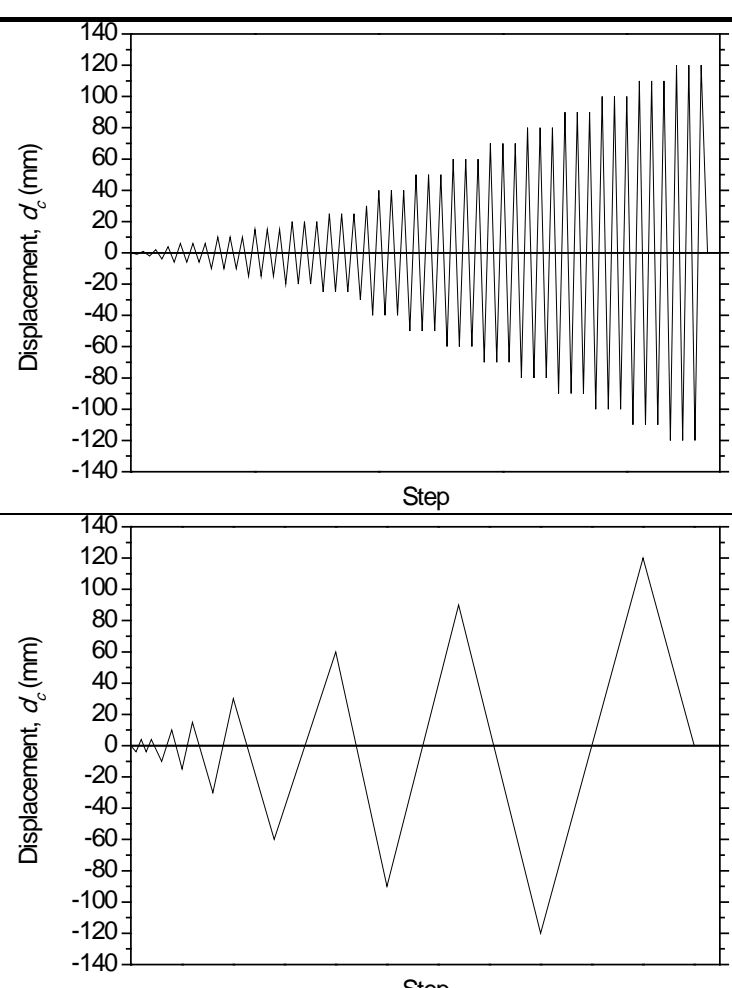


Figure 3 – Test setup: (a) General appearance of all the elements of the test setup; (b) Structural scheme obtained; (c) In situ photo.

The experimental program presented in this work was developed in two distinct phases. In a first one, the three RC joints were tested until failure according to the parameters presented on Table 1. Those parameters were defined according to the goals of another research project (Fernandes et al. 2011). In the following paragraphs the major aspects of the first phase are presented. The complete information can be found elsewhere (Fernandes et al. 2011).

Table 1 – Parameters for the tests in the first phase.

Specimen designation	Reinforcing steel type	Displacements law imposed at the top of the column ( $d_c$ )
JD	Ribbed	
JPA-1	Plain	
JPA-2		

As presented in this table, there were two joints with plain rebars and one with ribbed rebars.

Two different displacement laws were used. The first one consists on imposing complete cycles with signal inversion throughout eighteen displacement levels with growing amplitude. The levels chosen were  $\pm 1$  mm,  $\pm 2$  mm,  $\pm 4$  mm,  $\pm 6$  mm,  $\pm 10$  mm,  $\pm 15$  mm,  $\pm 20$  mm,  $\pm 25$  mm,  $\pm 30$  mm,  $\pm 40$  mm,  $\pm 50$  mm,  $\pm 60$  mm,  $\pm 70$  mm,  $\pm 80$  mm,  $\pm 90$  mm,  $\pm 100$  mm,  $\pm 110$  mm and  $\pm 120$  mm. From level  $\pm 1$  mm to  $\pm 4$  mm only one complete cycle per level was performed. From level  $\pm 6$  mm to the end of the test were performed three complete cycles per level. The second one consists on imposing complete cycles with signal inversion throughout seven displacement levels with growing amplitude. The levels chosen were  $\pm 4$  mm,  $\pm 10$  mm,  $\pm 15$  mm,  $\pm 30$  mm,  $\pm 60$  mm,  $\pm 90$  mm



and  $\pm 120$  mm. Only the  $\pm 4$  mm level was repeated twice, all the other levels had just one complete cycle.

Before the cyclic test begin, an axial force of 200 kN was applied at the top of the column. This force corresponds to a reduced axial force ( $u$ ) of about 10% which is a typical value for columns in buildings with 2-3 floors and spans with approximately 4 m. That force remains constant during the entire test of all the specimens.

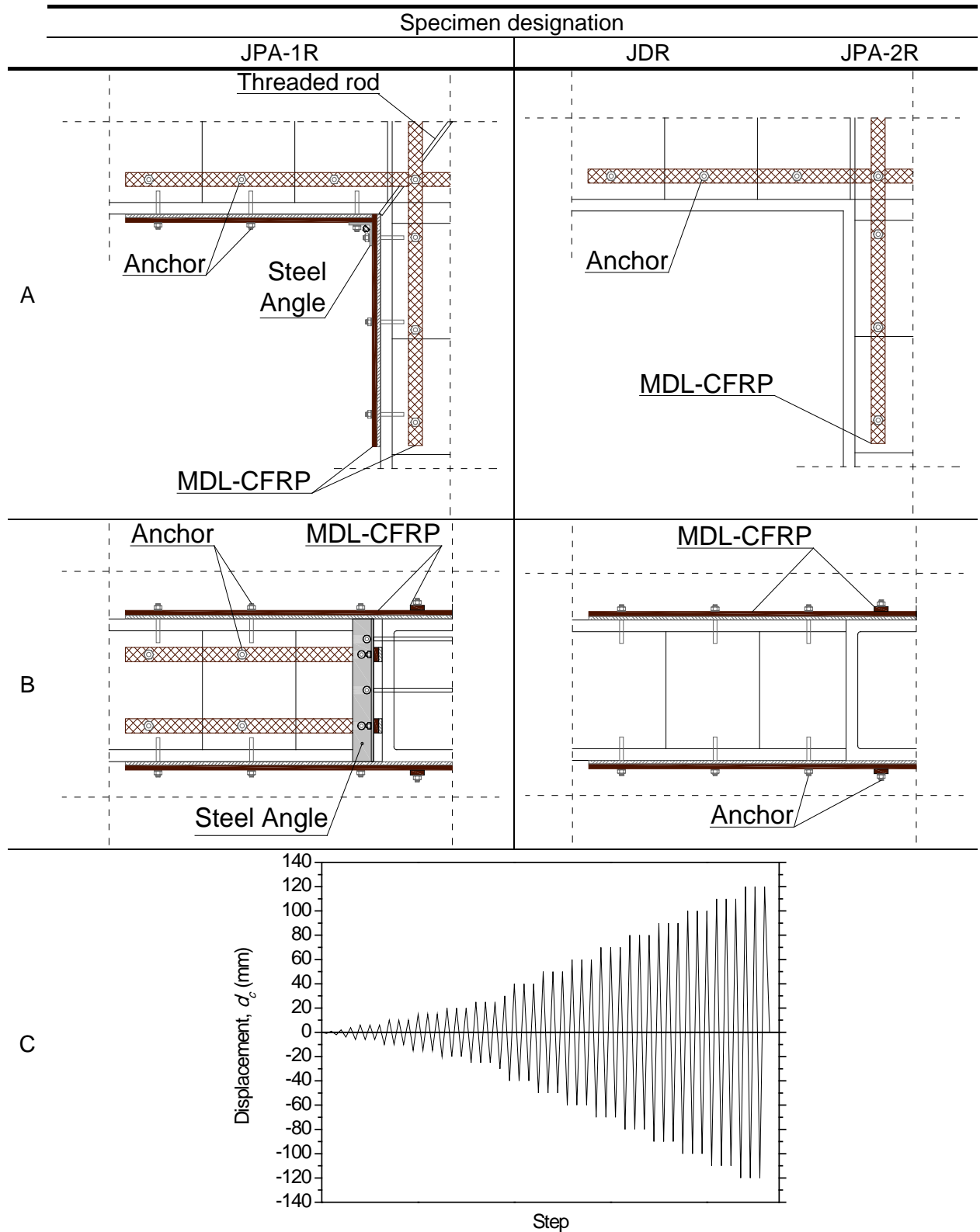
In all the tests of both phases, in the end of each displacement level, the tests were paused so it could be possible to check if new cracks arise and mark them with a marker.

On a second phase, all the joints were strengthened with MDL-CFRP according to the strengthening solutions defined in Table 2. In this second phase, the joints JD, JPA-1 and JPA-2 were designated as JDR, JPA-1R and JPA-2R.

The strengthening consists on attaching MDL-CFRP strips to the surface of the joints by the MF-EBR technique. There were two major solutions, one that was designated indirect strengthening, because the strips were only placed in the superior and inferior faces of the joint and the laminate was not working on its better direction, and one that was designated direct strengthening, because it had laminate strips on the lateral faces of the joint in addition to those placed on top and bottom faces like in the indirect strengthening. To guarantee that the strips on the lateral faces of the joint were connected, steel corners were used as can be seen in Table 2 and Figure 4. These were connected across the central region of the joint by 8 mm threaded rods.

The option for those two strengthening configurations was related with the real in situ conditions of a residential building. In the majority of the cases the indirect strengthening is the only viable option, but there can be some cases where the direct strengthening can be applied, so it was studied too in order to compare the results.

Table 2 – Strengthening solutions and test parameters for the second phase.



A – Strengthening configuration top view

B – Strengthening configuration side view

C – Displacements law imposed at the top of the column ( $d_c$ )

Figure 4 shows the global appearance of the complete solution (direct strengthening).

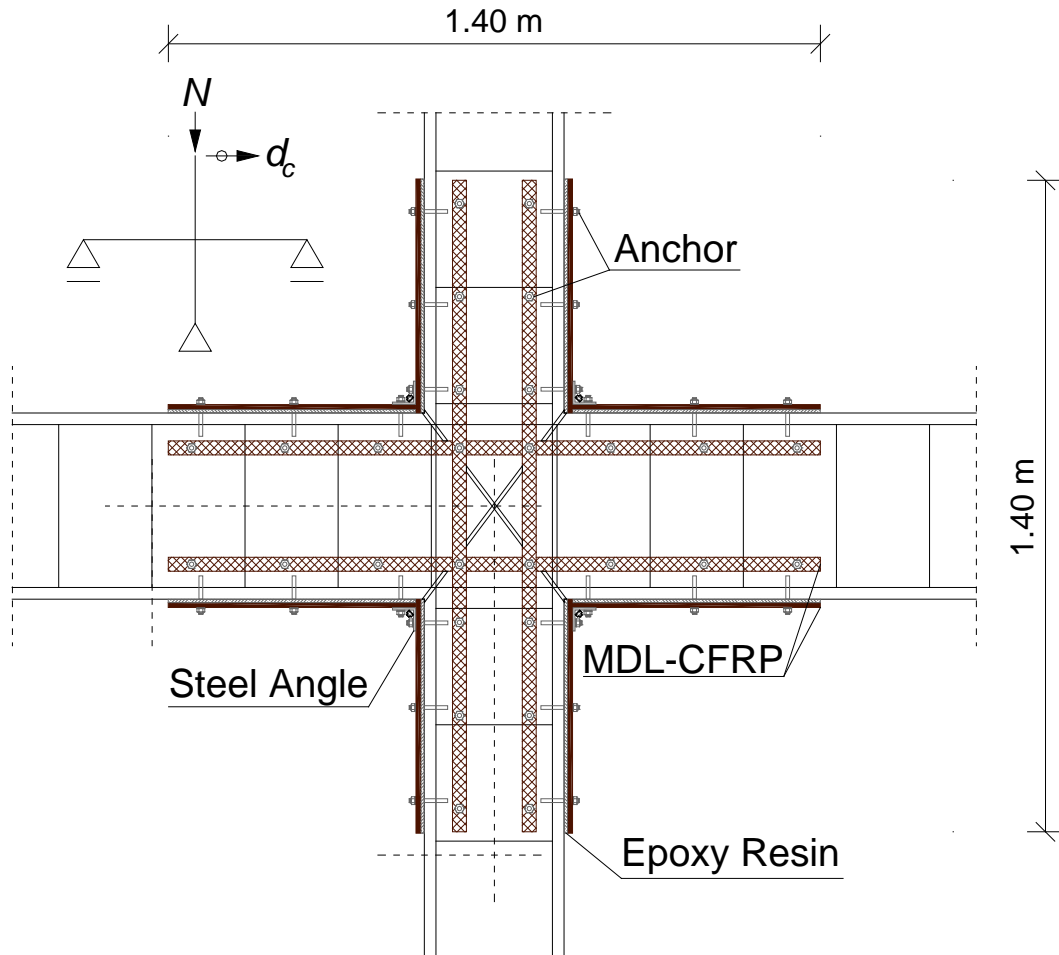


Figure 4 – Strengthening solution with MDL-CFRP.

In both phases all the tests were carried out under displacement control according to the load laws mentioned above. The load at the column top and the axial force on this were applied by two hydraulic servo-controlled actuators equipped with load cells of 200 kN (C1 in Figure 5) and 500 kN (C2 in Figure 5) capacity, respectively. Additionally two load cells were used. One with 300 kN of capacity to register the horizontal reaction at the base of the column (C3 in Figure 5) and other with 100 kN of capacity to register the vertical reaction at the same point (C4 in Figure 5).

The axial force was applied by C2 through a self-equilibrated system composed by two steel plates (at the top and the bottom of the column) and two steel bars parallel to the column as shown in Figure 3.



All the tests were monitored internal and externally. Figure 5 presents the location of the external instruments used. To register the behaviour of the specimens in the zones where the damage was expected to appear, eighteen potentiometers (P1-P18) were used. These register the approach or departure between the black spots where they were fixed. The horizontal displacements that were allowed in the beams supports were registered by two linear variable differential transducers (LVDT - L22 and L23). The displacement imposed at the top of the column was registered with more accuracy by the inductive linear position sensor (B1).

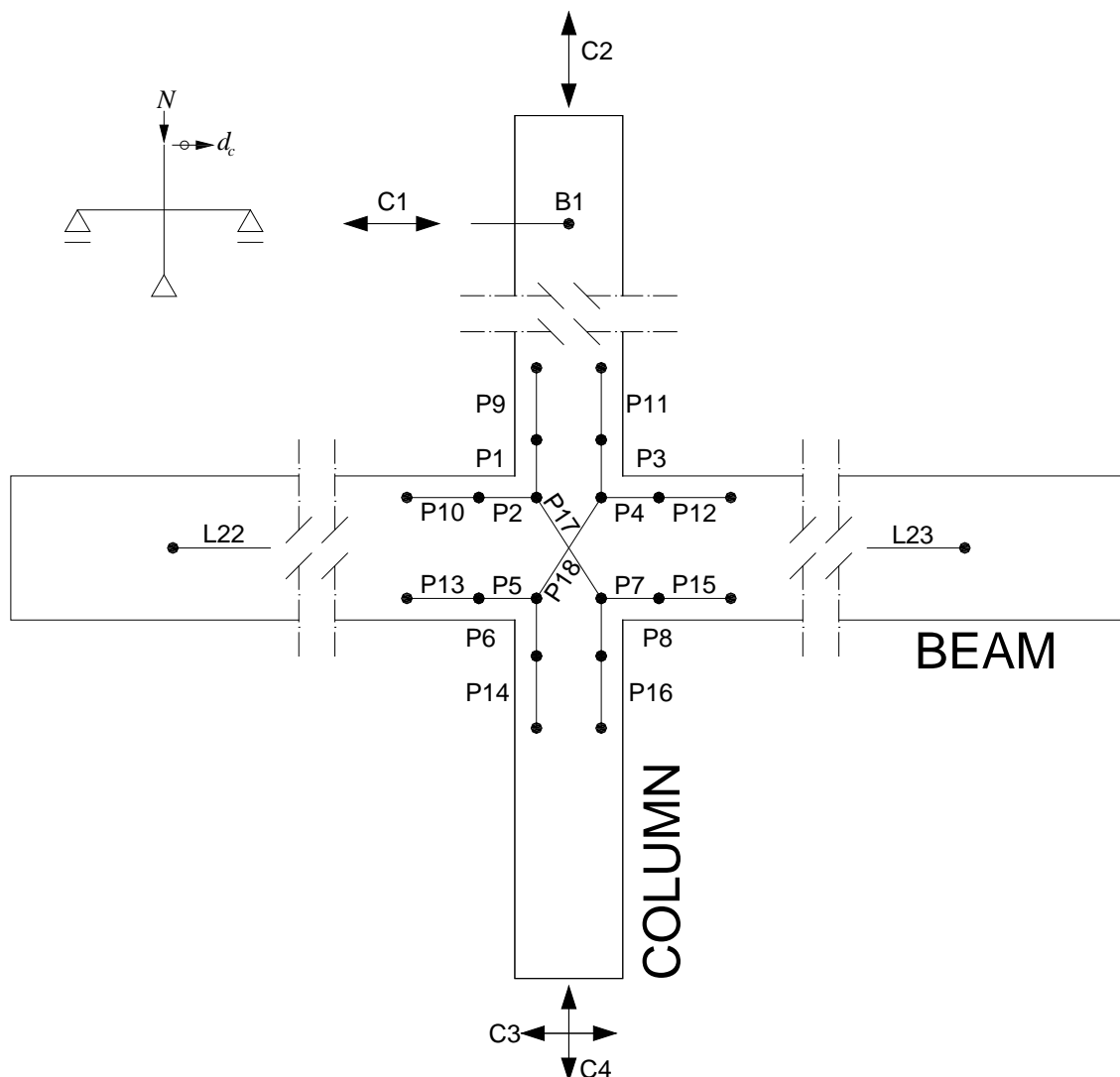


Figure 5 – Location of the external instrumentation used for monitoring the tests.

Figure 6 presents the location of the strain gauges (SG1-SG8) that were used only in the second phase of this work (strengthened specimens). These were located on the surface of the upper bar of each element (beam or column) at the indicated places.

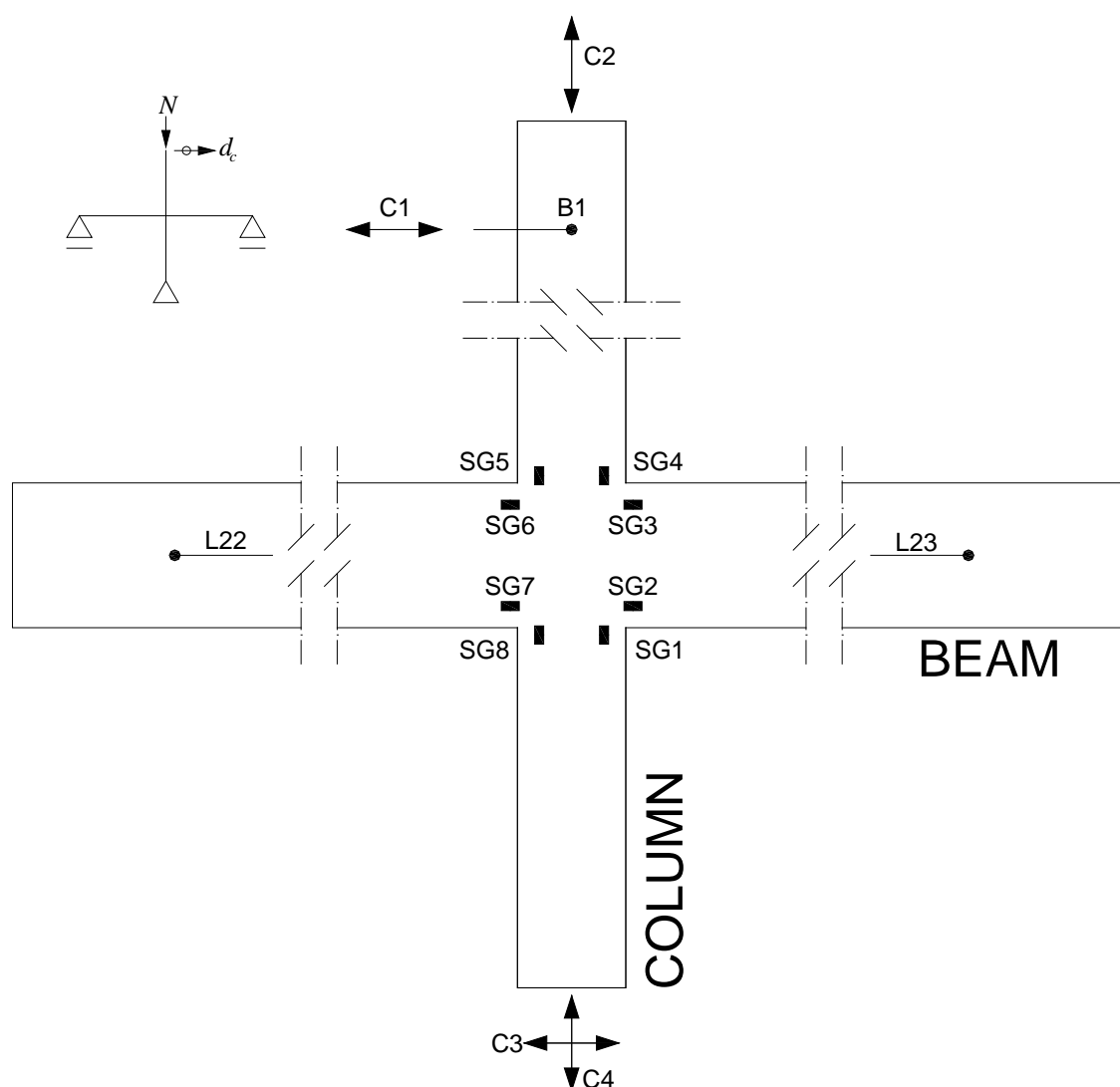


Figure 6 – Location of the strain gauges.

## 2.2 Material Characterization

The concrete used in this work was characterized by means of compressive tests in five cubic concrete specimens ( $15 \times 15 \times 15 \text{ cm}^3$ ) casted when the joints were casted too. An average compressive strength ( $f_{cm}$ ) of 23.5 MPa was obtained, which corresponds to a characteristic compressive strength ( $f_{ck}$ ) of 19.5 MPa, according to the specified on the EN 206-1:2000 + A1:2004 (PT). Based on this value and in the resistance classes defined in the referred standard and in the EN 1992-1-1:2004 (PT), it was concluded that the concrete class used to fabricate the joints was a C16/20.

The plain rebars properties were determined by means of tensile tests in bar samples according to EN 10 002-1:1990 (PT). The ribbed rebars properties were



assumed equal to those of normal A400 construction steel. Table 3 presents the mechanical properties of the two types of steel used in this work.

Table 3 – Mechanical properties of the rebars used in the joints.

Rebar	Property		
	Yielding stress $F_{s,ym}$ (MPa)	Ultimate stress $F_{s,um}$ (MPa)	Young modulus $E_s$ (GPa)
Plain	590	640	198
Ribbed	430	550	200

The multidirectional CFRP laminate (MDL-CFRP) used in the strengthening of the joints was designed and produced in the scope of the current research project. All the information related to its development and characterization can be consulted elsewhere (Sena-Cruz, 2010). Table 4 resumes the main properties of the MDL-CFRP.

Table 4 – MDL-CFRP properties.

Property	MDL-CFRP
Tensile strength (MPa)	1866
Elasticity modulus (GPa)	118
Failure strain (%)	1.58
Bearing unclamped resistance (MPa)	316
Bearing clamped resistance (MPa)	604
Thickness (mm)	2.07

To glue the MDL-CFRP to concrete an epoxy adhesive was used. The *S&P® Resin 220* was selected for this purpose. According to supplier, this resin has a flexural tensile strength, a compressive strength and bond concrete/laminate strength of 30 MPa, 90 MPa e 3 MPa, respectively.

To mechanically fix the MDL-CFRP to concrete a Hilti® chemical anchors system was adopted to fix mechanically the laminate to concrete. This system is composed by the resin HIT-HY 150 MAX, the HIT-V M8 8.8 threaded anchors and DIN 9021 washers. The anchors were pre-stressed using a torque of 40 Nxm. This value was defined based on preliminary tests that were carried with the same materials.

## 2.3 Specimens Preparation

The preparation of the nodes involved three main steps. The following paragraphs present the multiple tasks that compose each of these steps.

Before initiating the preparation of the joints, they were turned so the retrofit work began by the inferior face and, after this face has been treated, the joint was again turned to the initial position to be tested. The rotation of the joints was performed with the aid of solid wood squares placed in order to minimize the opening of the cracks, before and after sealing them. Figure 7 shows an informative picture of the joints rotation.



Figure 7 – Joint rotation.

### **Joint reconstruction**

After the first phase tests the joints presented several damages especially in the central zone. So, the first step was to reconstruct that zone of the joints. This process involved the following main tasks:

- a) Removal of deteriorated concrete in the corners area of the node and then cleaning with compressed air;
- b) Application of the formwork (Figure 8a);
- c) Preparation of the grout used in the reconstruction (Figure 8b);
- d) Filling the formwork with grout (Figure 8c);
- e) Surface regularization (Figure 8d).

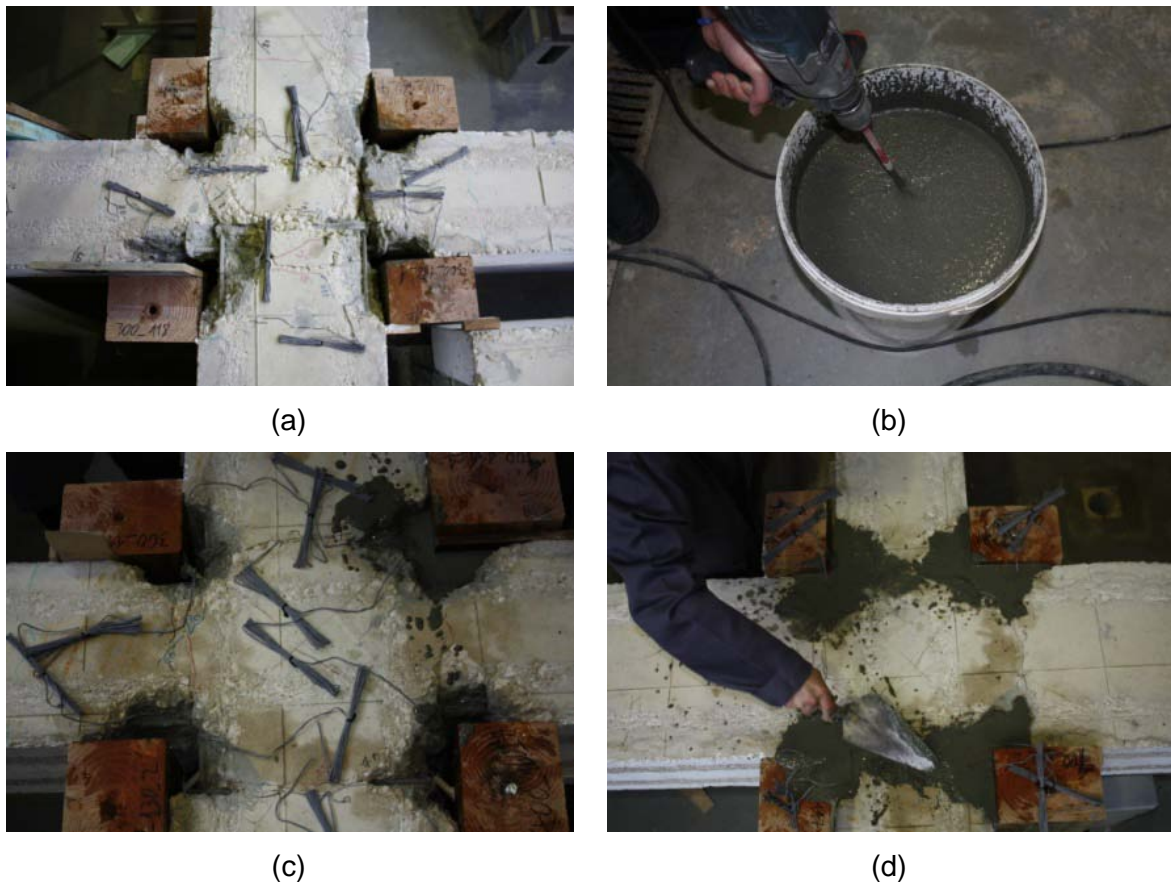


Figure 8 – Joint reconstruction: (a) formwork; (b) grout preparation; (c) filling the formwork with grout; (d) surface regularization.

As can be seen in Figure 8c, referring to JPA-1R joint, 12 mm diameter tubes were placed in this joint at its diagonals. The purpose of these tubes was to act as a negative for the threaded 8 mm diameter rods that would connect the corner metal elements which were later put in this joint in order to give continuity to the MDL-CFRP placed on the sides of this joint.

As can also be seen in Figure 8, in this step eight strain gauges were glued to the steel reinforcement according to the positions defined in Figure 5.

### **Cracks sealing**

Even though the reconstruction of the joint has replaced the material that was lost during the first phase tests it was not able to close the micro cracks that existed in the concrete. That was accomplished in another step that can be called cracks sealing. The cracks sealing had essentially two goals, on one hand to bond the old concrete in the slit area and, on the other, to bond the old concrete to the new grout in the reconstructed areas. That step involved the following main tasks:

- a) Removal of the formwork after the grout being cured (Figure 9a);
- b) Drilling of boreholes in the area of the cracks (through them) to place purges in all the faces of each element (beam or column), except on the underside. These purges were materialized by small transparent hoses;
- c) Sealing the areas of the cracks and around the purges with iron mass to prevent the resin to escape (Figure 9b);
- d) Injection of the resin through the purges (Figure 9c). This process began by side purges of each element and finished when the superior purge of that element started to lose resin, meaning that it had already filled the entire slit. The resin used for this purpose was the one showed in Figure 9a.



(a)



(b)



(c)



(d)

Figure 9 – Sealing the cracks: (a) formwork removal; (b) cracks sealing, with iron mass and purges application; (c) injection of the sealing resin; (d) final appearance of the joint after sealing the cracks.



### **MDL-CFRP application**

The last step of the strengthening was the application of the MDL-CFRP. This step involved the following main tasks:

- a) Creation of a roughness on the concrete surface, using a needle hammer, followed by cleaning this with compressed air (Figure 10a);
- b) Cleaning the MDL-CFRP with acetone;
- c) Placement of epoxy adhesive on the concrete surface and on the laminate surface that would be in contact with it;
- d) Placement of the laminate on the concrete surface, pressing it slightly against this in order to create a uniform thickness of adhesive of 1-2 mm;
- e) Removal of the epoxy adhesive in excess;
- f) After epoxy cure (1 day at least), marking the sites of the holes on the face of the MDL-CFRP with the aid of a steel detector;
- g) Drilling holes with 10 mm diameter and 100 mm depth with a diamond coring system and a drill stand to ensure verticality of the holes;
- h) Cleaning the holes with compressed air and a steel brush;
- i) Filling the holes with chemical adhesive HIT-HY 150 MAX, followed by placement of the screws on these, to a depth of 100 mm.



(a)



(b)

Figure 10 – MDL-CFRP application: (a) Creation of roughness on the concrete surface; (b) appearance of the treated area where the laminate would be glued.

In the case of JPA-1R joint this process was repeated in the side faces of each element (beam or column).



### 3 RESULTS

In this section the main results of the tests performed on the retrofitted joints are presented and compared to those obtained in the first phase of tests. The results of the first phase tests can be consulted elsewhere (Fernandes et al. 2011).

For all the specimens, the first cycle at each load step was the one that presented higher force values.

After performing the same cycles that JD specimen has accomplished, JDR test has done two more cycles at a displacement level of  $\pm 150$  mm. JPA-1R specimen test went to the second cycle of step  $\pm 110$  mm. JPA-2R has accomplished two cycles at step  $\pm 150$  mm and one at step  $\pm 190$  mm. At those moments, the behaviour of the specimens was too instable and the tests were stopped for safety reasons.

The results that do not appear in this section can be consulted in the respective appendix at the end of this report. Examples of this are the forces registered by the load cells C2, C3 and C4, the displacements registered by the elements P1-P18, L22-L23 and B1.

#### 3.1 Displacement *versus* Force

Figure 11 presents the relationship between the displacement and the force registered by load cell C1 (lateral force) for all the specimens. The corresponding envelopes are also presented.

Table 5 presents the main obtained results. As it can be seen, JDR and JPA-1R present high values of maximum force in both ways of test then JD and JPA-1, respectively.

In the case of specimens JPA-2 and JPA-2R that is not verified. It can even be said that the envelopes are quite similar, being the JPA-2 maximum force marginally higher than the JPA-2R.

In JD specimens, the maximum force was obtained for an earlier displacement level in the unreinforced specimen while, in JP specimens, the maximum force was obtained for an earlier displacement level in the reinforced ones.



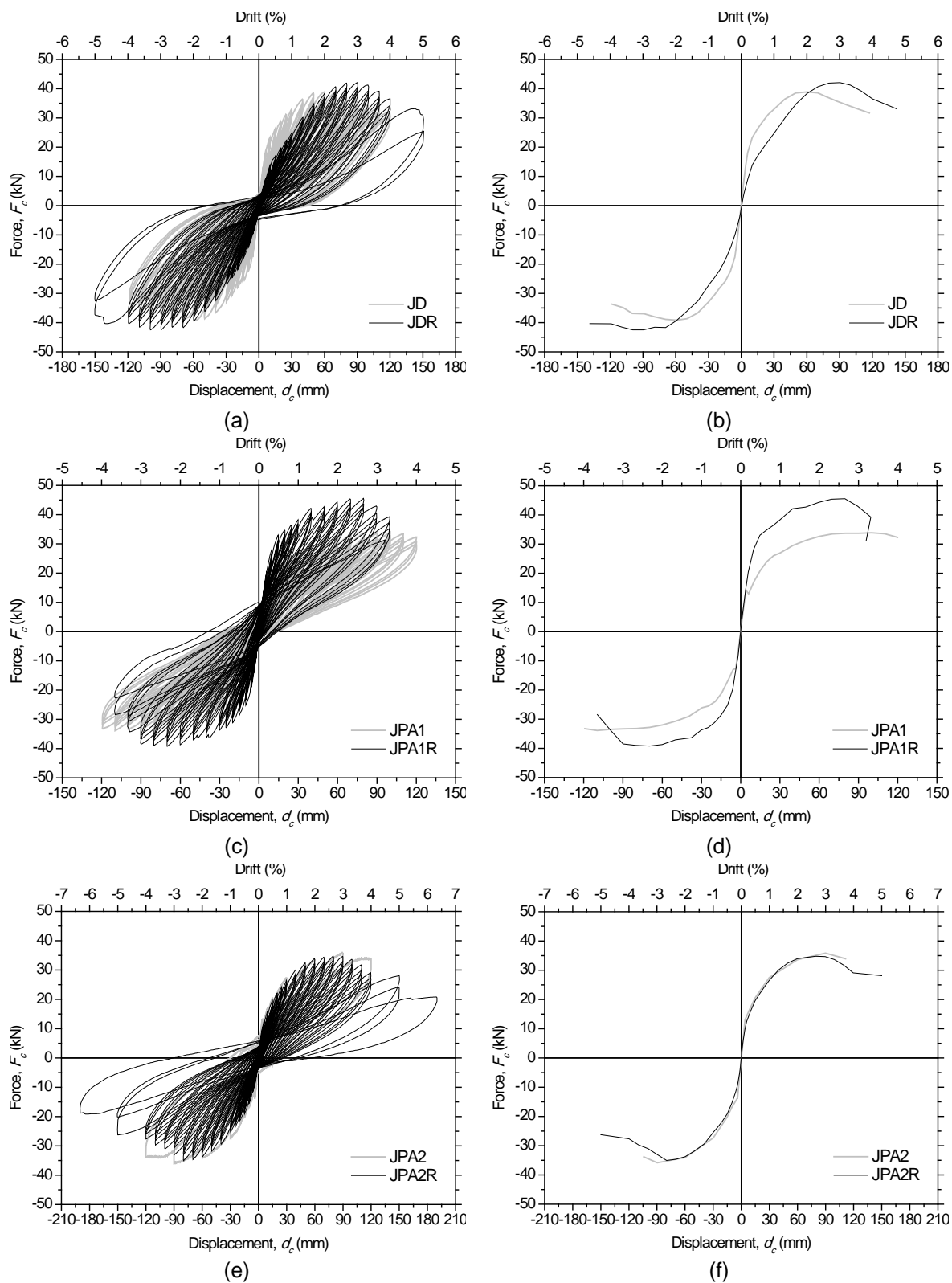


Figure 11 – Displacement versus Force registered by load cell C1: (a) JD and JDR; (b) JD and JDR envelopes; (c) JPA-1 and JPA-1R; (d) JPA-1 and JPA-1R envelopes; (e) JPA-2 and JPA-2R; (f) JPA-2 and JPA-2R envelopes.

Table 5 – Maximum forces registered by load cell C1.

Specimen	Negative branch		Positive branch	
	$F_{c,max}$ (kN)	Cycle	$F_{c,max}$ (kN)	Cycle
JD	-39.14	-60	38.9	-60
JDR	-42.48 (9%)	-100	42.11 (8%)	-90
JPA-1	-33.85	-110	33.85	-100
JPA-1R	-39.22 (16%)	-70	45.54 (35%)	-80
JPA-2	-35.85	-90	35.84	-90
JPA-2R	-35.06 (-2%)	-80	34.78 (-3%)	-80

Note: The values in brackets represent the increase from the original to the strengthened specimens.

In order to have a comparison rule between the results of all the tests, the envelopes presented in Figure 11 were used to estimate an idealized elasto-perfectly plastic force–displacement relationship. The determination of this relationship was performed according to the methodology prescribed in the Annex B of EN 1998-1:2004(E). Figure 12 presents a graphical view of the type of approximation methodology referred. Transposing for the present study case, point A coincides with the maximum force point in each cycle, being  $(d_m^*, F_y^*)$  its coordinates. The parameter  $E_m^*$  is the actual deformation energy up to point A. The only unknown point is the yield displacement of the idealized curve. This point can be calculated by the following equation:

$$d_y^* = 2 \left( d_m^* - \frac{E_m^*}{F_y^*} \right) \quad (1)$$

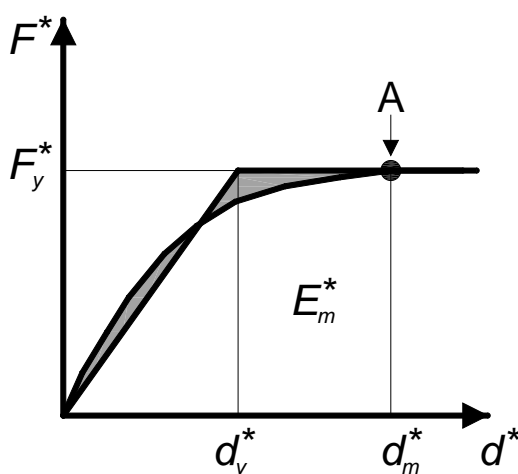


Figure 12 – Determination of the idealized elasto-perfectly plastic force versus displacement relationship (adapted from EN 1998-1:2004 (E)).

Figure 13 presents a comparison between the original envelopes and the idealized elasto-perfectly plastic curves for each specimen.

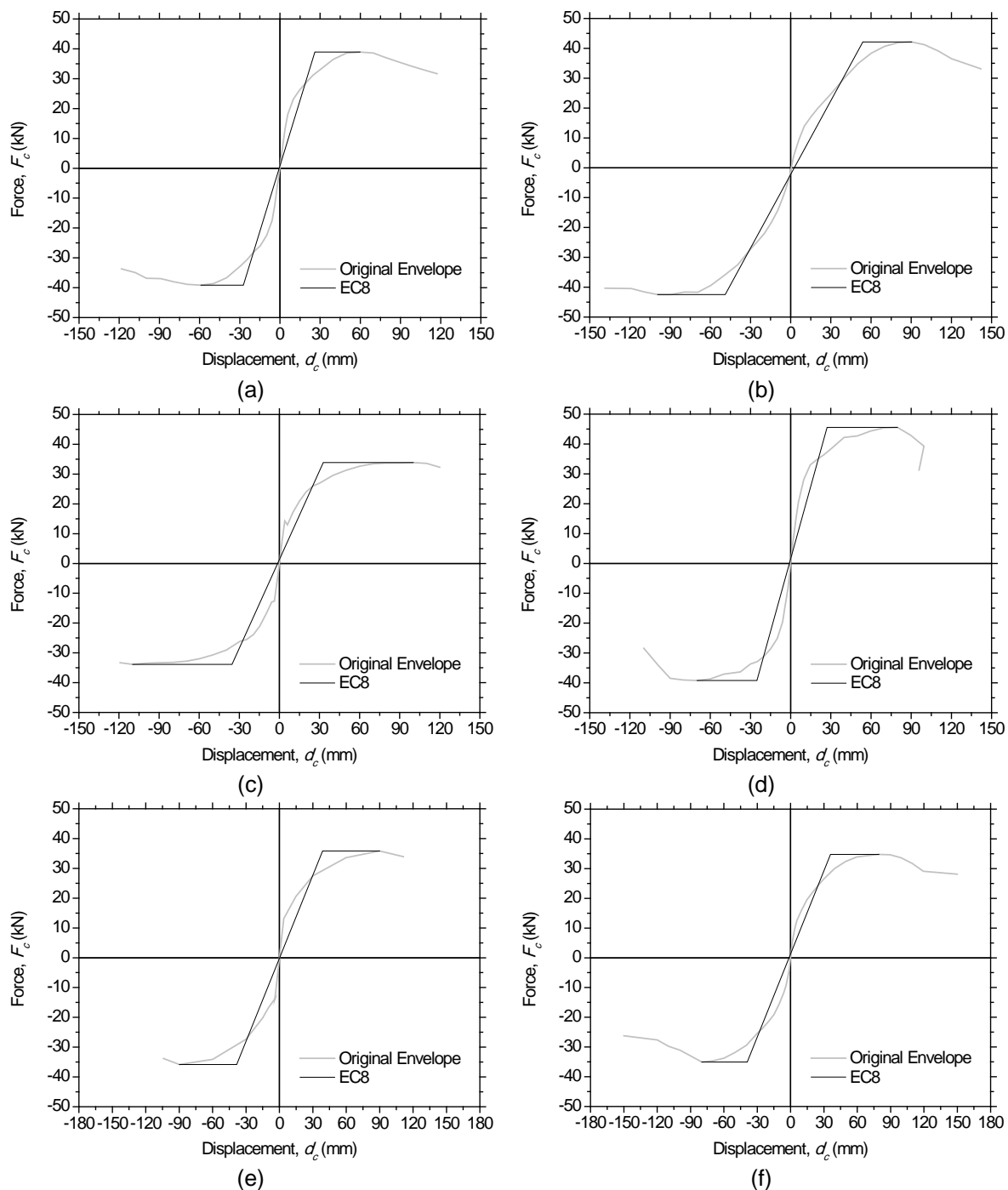


Figure 13 – Displacement ductility: (a) JD; (b) JDR; (c) JPA-1; (d) JPA-1R; (e) JPA-2; (f) JPA-2R.



Table 6 presents the values that were used to define the displacement ductility. In this table,  $d_y^-$  and  $d_y^+$  represent the yielding displacement in the idealized elasto-perfectly plastic curve at the negative and positive branch, respectively, while  $d_u^-$  and  $d_u^+$  represent the ultimate displacements, in the same curves, at the negative and positive branch, respectively.

Assuming displacement ductility as the ratio  $(d_u^- + d_u^+) / (d_y^- + d_y^+)$ , Table 6 gives a comparison of that value between unreinforced and reinforced specimens. The values in brackets represent the decrease in ductility from the unreinforced to the respective reinforced specimen.

Table 6 – Displacement ductility of JD specimens.

Specimen	$d_y^-$	$d_u^-$	$d_y^+$	$d_u^+$	$(d_u^- + d_u^+) / (d_y^- + d_y^+)$
JD	-27.26	-59.04	26.04	59.81	2.23
JDR	-48.83	-99.28	53.83	90.30	1.85 (-17%)
JPA-1	-35.46	-109.72	32.82	100.13	3.07
JPA-1R	-25.15	-69.76	27.21	79.68	2.85 (-7%)
JPA-2	-38.30	-89.73	38.77	89.98	2.33
JPA-2R	-39.02	-79.80	35.90	79.55	2.13 (-9%)

According to the obtained results, it can be said that all the reinforced specimens had less displacement ductility than the unreinforced specimens, being this difference more expressive in the case of the ribbed rebars specimens.

### 3.2 Dissipated Energy

Figure 14 shows the evolution of the dissipated energy along the drift levels of the tests. In this case, because the columns had 3 m length, 1% of drift corresponds to a displacement level of  $\pm 30$  mm. The dissipated energy was calculated using the trapezium rule to estimate the area under the curves presented in Figure 11 (not the envelopes).

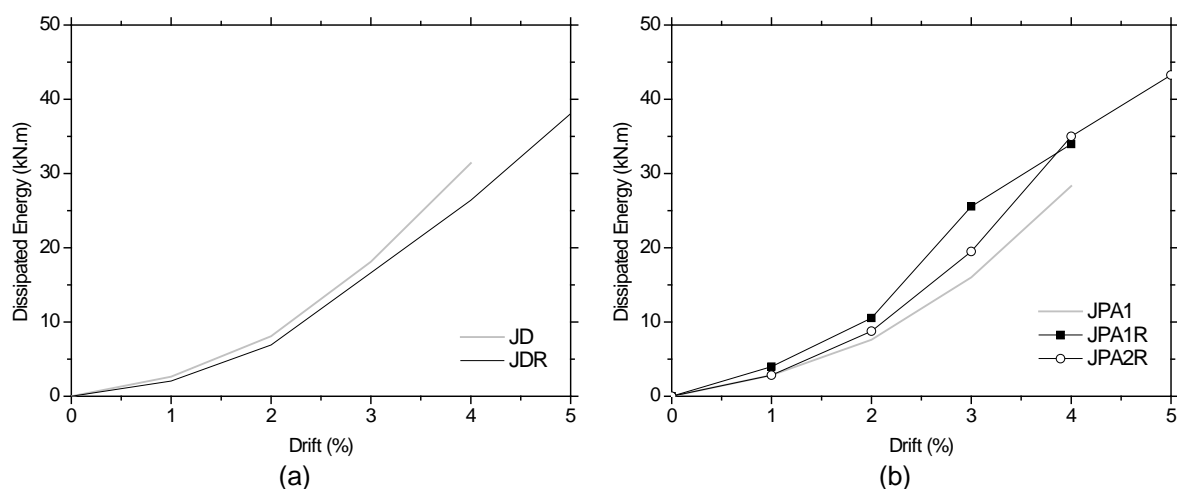


Figure 14 – Dissipated energy: (a) JD/JDR; (b) JPA-1/JPA-1R/JPA-2R.

Until the drift level of 4%, corresponding to the step  $\pm 120$  mm, JD as dissipated more energy than JDR.

Because the displacement law in JPA-2 specimen in the first phase of tests was different than the one used for all joints in the second phase, the results of this specimen were compared to those of the JPA-1 specimen. In fact, JPA-1 and JPA-2 specimens have the same structural characteristics so this comparison is acceptable.

In terms of dissipated energy, both reinforced joints present higher values than the unreinforced one, being the JPA-1R the one that dissipates more energy.

Table 7 presents a numerical view of the results plotted in Figure 14.

Table 7 – Dissipated Energy of JD specimens.

Drift (%)	Dissipated Energy (kN.m)				
	JD	JDR	JPA1	JPA1R	JPA2R
1	2.65	2.06 (-22%)	2.84	3.98 (40%)	2.83 (-1%)
2	8.08	6.90 (-15%)	7.63	10.54 (38%)	8.75 (15%)
3	18.13	16.64 (-8%)	16.02	25.56 (60%)	19.49 (22%)
4	31.42	26.39 (-16%)	28.32	33.96 (20%)	34.99 (24%)
5	-	38.05	-	-	43.26

The curves of the dissipated energy for each specimen were calculated using the values that are included in Table 7, which represent the cumulative dissipated energy for each drift level. Besides, in the column of the reinforced specimens, the percentage of decrease compared to the respective unreinforced ones, is presented in brackets.

### 3.3 Stiffness

Figure 15 presents the stiffness degradation of the specimens along the cycles. This stiffness was assumed to be secant stiffness and was calculated as the slope of the line that can be drawn between the maximum positive and negative force point in each half cycle of the curves presented in Figure 11 (not the envelopes). It's an approximation but it gives a qualitative measure to compare the stiffness degradation between the specimens.

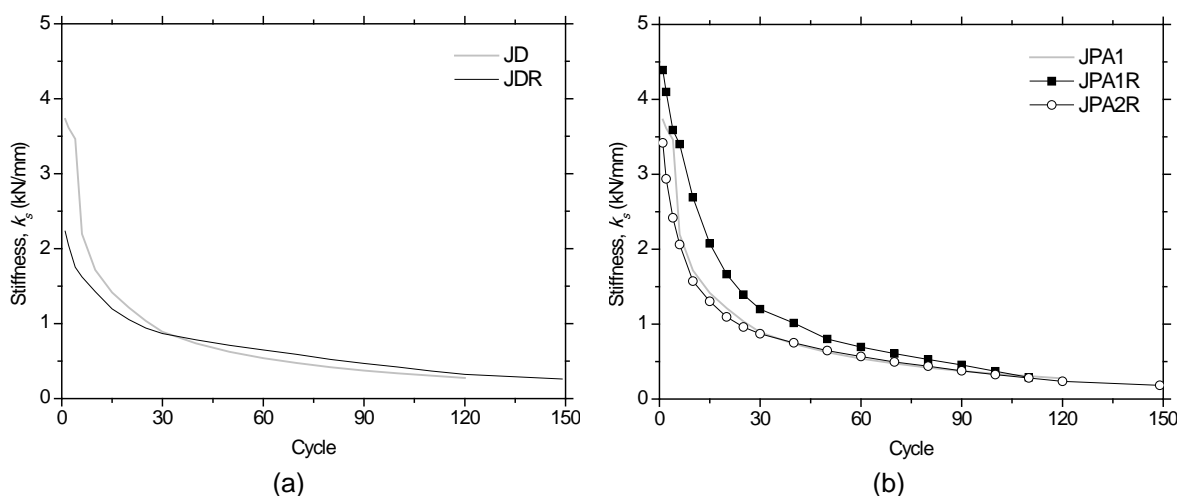


Figure 15 - Stiffness degradation: (a) JD/JDR; (b) JPA-1/JPA-1R/JPA-2R.

Specimen JD presents higher initial secant stiffness ( $k_{s,0} = 3.33$  kN/mm) than JDR ( $k_{s,0} = 2.23$  kN/mm). Regarding to the plain rebars specimens, JPA-1 has higher initial secant stiffness ( $k_{s,0} = 3.73$  kN/mm) than JPA-2R ( $k_{s,0} = 3.42$  kN/mm) but lower than JPA-1R ( $k_{s,0} = 4.39$  kN/mm).

When calculating the initial stiffness as the slope of the initial linear branch of the curves displacement versus force presented in Figure 11 (not the envelopes), we obtain  $k_0 = 3.20$  kN/mm (-4.1% than  $k_{s,0}$ ),  $k_0 = 1.95$  kN/mm (-14.4% than  $k_{s,0}$ ),  $k_0 = 3.38$  kN/mm (-10.4% than  $k_{s,0}$ ),  $k_0 = 4.20$  kN/mm (-4.5% than  $k_{s,0}$ ) and  $k_0 = 3.19$  kN/mm (-7.2% than  $k_{s,0}$ ) for specimens JD, JDR, JPA-1, JPA-1R and JPA-2R, respectively.

### 3.4 Strains

Figure 16 presents the results obtained by the strain gauges (SG) that were glued on the internal steel reinforcement of the strengthened specimens (see Figure 6).

In JDR specimen the SG2 and SG5 became damaged near the end of the level  $\pm 150$  mm and  $\pm 80$  mm, respectively.

For the case of JPA-1R joint, the SGs that stopped working before the end of the test were SG1, SG6, SG7 and SG8. Those have all stop reading at the end of the level  $\pm 60$  mm.

Finally, in JPA-2R test, SG2, SG5 and SG6 stop reading at the levels  $\pm 20$  mm,  $\pm 150$  mm and  $\pm 90$  mm, respectively, while SG7 and SG8 stop reading at level  $\pm 25$  mm.

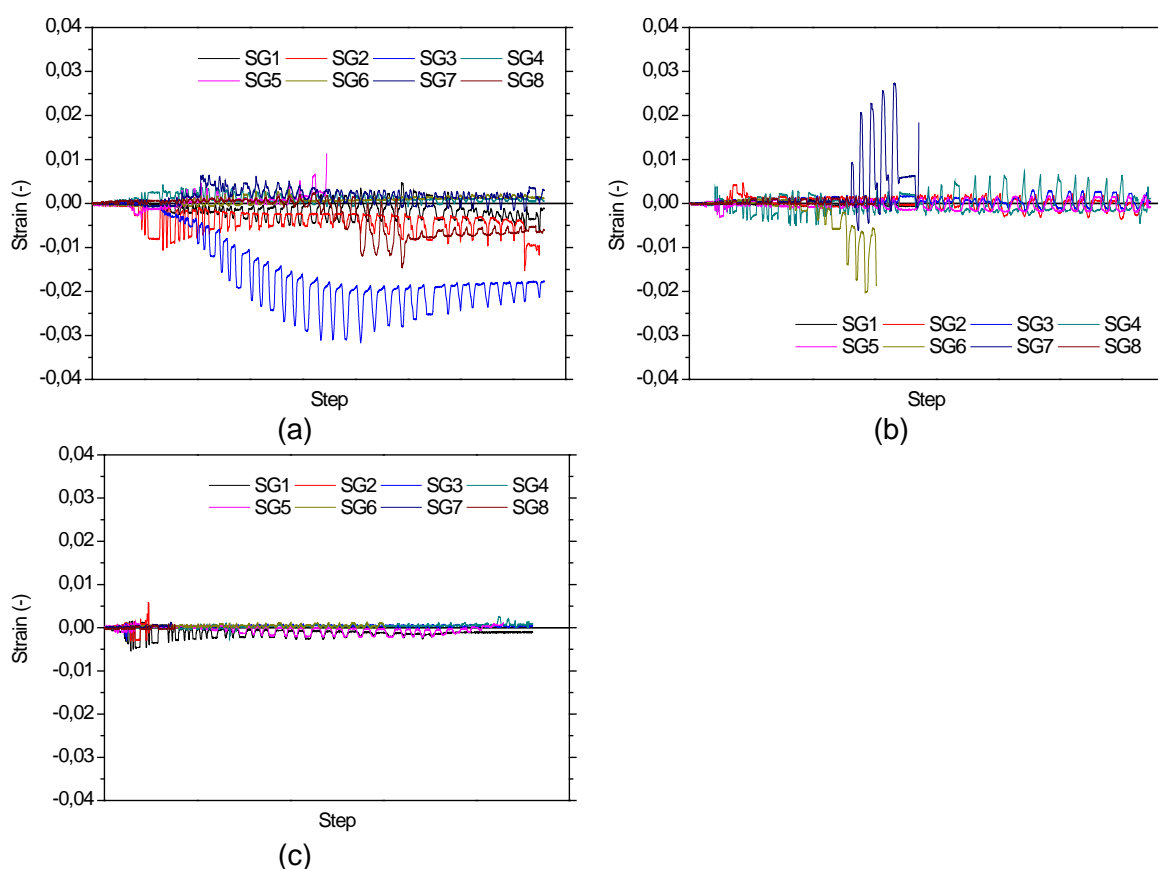


Figure 16 – Strain results (a) JDR specimen test; (b) JPA-1R specimen test; (c) JPA-2R specimen test.

Assuming the steel properties presented in Table 3, it can be said that no steel yielding occurred in all the tests. The exception to this fact is the steel bar in which SG7 was glued that present a strain value beyond the yielding strain of the ribbed rebars.

### 3.5 FAILURE MODES

Figure 17 shows the damage in the strengthened specimens at the end of the corresponding test. As can be seen, the damage was higher in JDR specimen and lower in JPA-1R. The steel corners existent in this last one have actually helped a lot to this as they prevented the concrete detachment to be so pronounced as the one seen in JDR and JPA-2R specimens.

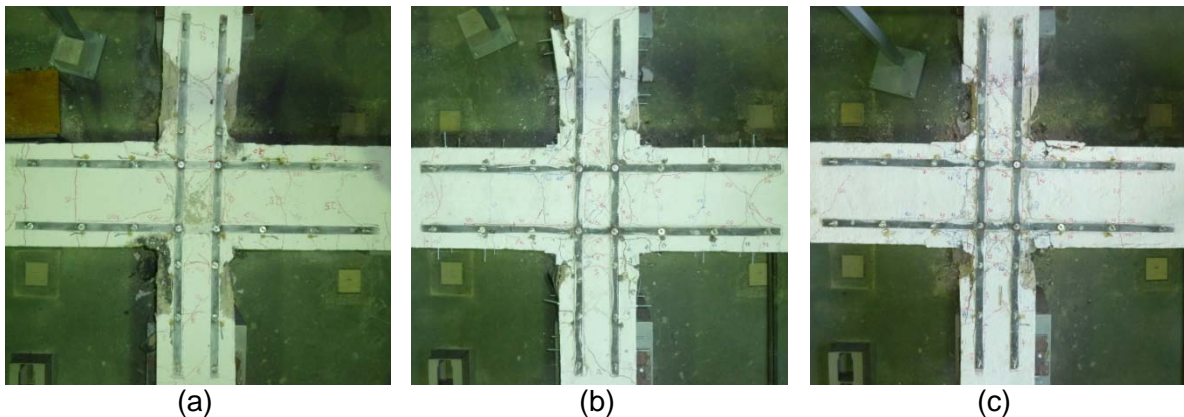


Figure 17 – Damage in the joints after the tests: (a) JDR; (b) JPA-1R; (c) JPA-2R.

JDR crack initiation occurred at level  $\pm 6$  mm and  $\pm 15$  mm in the beams and columns, respectively, while crack initiation occurred at level  $\pm 10$  mm and  $\pm 4$  mm in the beams of JPA-1R and JPA-2R specimens, respectively. In the columns, crack initiation occurred at level  $\pm 10$  mm for both specimens.

The results obtained by the potentiometers that were located at the centre of each specimen give us an idea of the damage development. Those results, which can be seen in the Annexes II to IV, show that, for all the specimens, the biggest displacements occur in the middle of the joint, then in the potentiometers located in the column and after that in the ones located in the beam. In each element (beam or column) the displacements are higher in the potentiometer closest to the centre of the specimen.

## 4 CONCLUSIONS

In terms of displacement versus force relationship, JDR and JPA-1R presented higher values of maximum force in both ways of test than JD and JPA-1, respectively, while JPA-2R presented lower maximum force in both ways.





In JD specimens, the maximum force was obtained for an earlier displacement level in the unreinforced specimen while, in JP specimens, the maximum force was obtained for an earlier displacement level in the reinforced ones. That fact probably is directly related to the fact of the slip between the ribbed rebars and concrete be much lower than the slip between plain rebars and concrete. One of the functions of the MDL-CFRP was to delay the opening of cracks. In the case of JD specimens the help given by MDL-CFRP was not so expressive because the bond between the ribbed rebars and concrete was already high. In the case of plain rebars specimens these function of MDL-CFRP was much more expressive.

Before being reinforced, ribbed rebars specimen JD had dissipated more energy than plain rebars specimen JPA-1, but, after being reinforced with MDL-CFRP, plain rebars specimens (JPA-1R and JPA-2R) dissipated more energy than the ribbed rebars one (JDR). Between JPA-1R and JPA-2R, the first one had dissipated more energy than the second one. That was expected because JPA-1R had more strengthening material and it was applied in a more effective way.

In terms of stiffness degradation, JDR and JPA-2R presented similar values than the respective unreinforced specimens while JPA-1R presented higher values along the entire test than JPA-1.

In general, the results show that the initial properties of the joints were almost recovered, but the improvements beyond these were not so significant.

The explanation to that fact could be associated to a bad joint reconstruction, especially at the crack sealing phase, or just to an inadequate or insufficient reconstruction work compared to the initial damage of the specimen.

More work needs to be done in this field with more specimens and more strengthening solutions. Also, the introduction of non-damaged specimens in future test campaigns can be very useful in order to see the actual improvements that the strengthening can give.

## 5 ACKNOWLEDGMENTS

This work is supported by FEDER funds through the Operational Programme for Competitiveness Factors – COMPETE and National Funds through FCT – Portuguese Foundation for Science and Technology under the project PTDC/ECM/74337/2006. The authors acknowledge the materials generously supplied by Hilti Portugal - Produtos e



Serviços Lda., S&P Clever Reinforcement Ibérica Lda. and SECIL, and TSwaterjet, Lda. for cutting of the laminates using the water-jet technology.

## 6 REFERENCES

- American Concrete Institute (ACI), (2008). "Guide for the design and construction of externally bonded FRP systems for strengthening concrete structures." Report ACI 440.2R-08 by ACI Committee 440, Farmington Hills, USA, 80 pp.
- Bakis, C. E., Bank, L. C., Brown, V. L., Cosenza, E. Davalos, J., Lesko, J. J., Machida, A., Rizkalla, S., and Triantafillou, T. (2002). "FRP Composites for Construction - State of the Art Review," J. Composites for Construction, 6:73-87.
- Bank, L.C. (2004). "Mechanically Fastened FRP (MF-FRP) Strips for Strengthening RC Structures – A Viable Alternative", Proceedings of CICE 2004, 2nd International Conference on FRP Composites in Civil Engineering, December 8-10, Adelaide, Australia, 12 pp.
- Barros, J.A.O., Fortes, A. (2005). "Flexural strengthening of concrete beams with CFRP laminates bonded into slits." Cement and Concrete Composites, 27(4), 471-480.
- CNR-DT 200 (2004). "Guide for the Design and Construction of Externally Bonded FRP Systems for Strengthening Existing Structures." National Research Council, Rome, 157 pp.
- Lopes, M. et al. (2008). "Sismos e Edifícios", Orion Editions, ISBN: 978-972-8620-11-0 (in Portuguese).
- Mukherjee, A., Joshi, M. (2005). "FRPC reinforced concrete beam-column joints under cyclic excitation", Composite Structures 70, 185–199.
- Engindeniz, M., Kahn, L.F., Zureick, A., (2004) "Repair and Strengthening of Non-Seismically Designed RC Beam-Column Joints: State-of-the-Art", Georgia Institute of Technology, School of Civil and Environmental Engineering, Structural



Engineering, Mechanics and Materials, Research Report No. 04-4, pp.59, October 2004.

Fernandes, C., Melo, J., Varum, H., Costa, A. (2011). Comparative analysis of the cyclic behaviour of beam-column joints with plain and deformed reinforcing bars - Revista IBRACON de Estruturas e Materiais, RIEM, Volume 4, Number 1-March, p. 147-172, ISSN 1983-4195.

EN 206-1:2000 + A1:2004 (PT). "Concrete Part 1: Specification, performance, production and conformity", 2005

EN 1992-1-1:2004 (PT). "Eurocode 2: Design of concrete structures - Part 1-1: General rules and rules for buildings." CEN, Brussels, 2010.

EN 1998-1:2004 (E). "Eurocode 8: Design of structures for earthquake resistance - Part 1: General rules, seismic actions and rules for buildings." CEN, Brussels, 2004.

EN 10 002-1:1990 (PT). "Metallic materials - Tensile testing. Part 1: Method of test (at ambient temperature)". CEN, Brussels, Belgium, 35 pp., November 1990.

Ray, J. C., Scott, D. W., Lamanna, A. J., and Bank, L. C. (2000). "Flexural behavior of reinforced concrete members strengthened using mechanically fastened fiber reinforced polymer plates." Proc., 22nd Army Science Conf., The United States Army, Washington, D.C., 556–560.

Sena Cruz, J.M., Barros, J.A.O., Coelho, M. (2010). "Bond Between Concrete and Multi-Directional CFRP Laminates." Advanced Materials Research - Structural Analysis of Historic Constructions, Vols. 133-134, 917-922.

[doi:10.4028/www.scientific.net/AMR.133-134.917]

# **ANNEX I**

---

## **INSTRUMENTATION LOCATION**

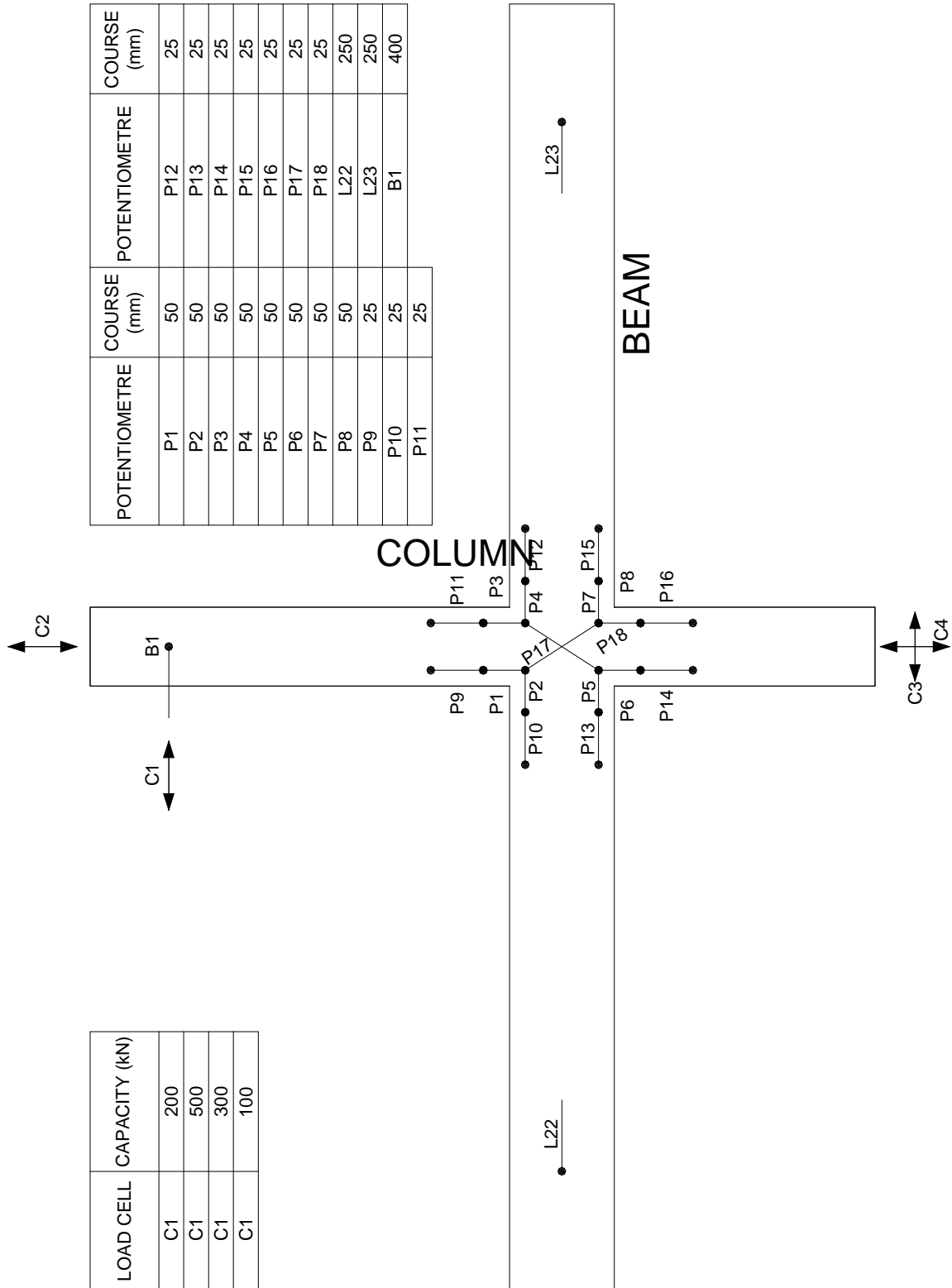


Figure I.1 – Location of the instrumentation for monitoring tests.

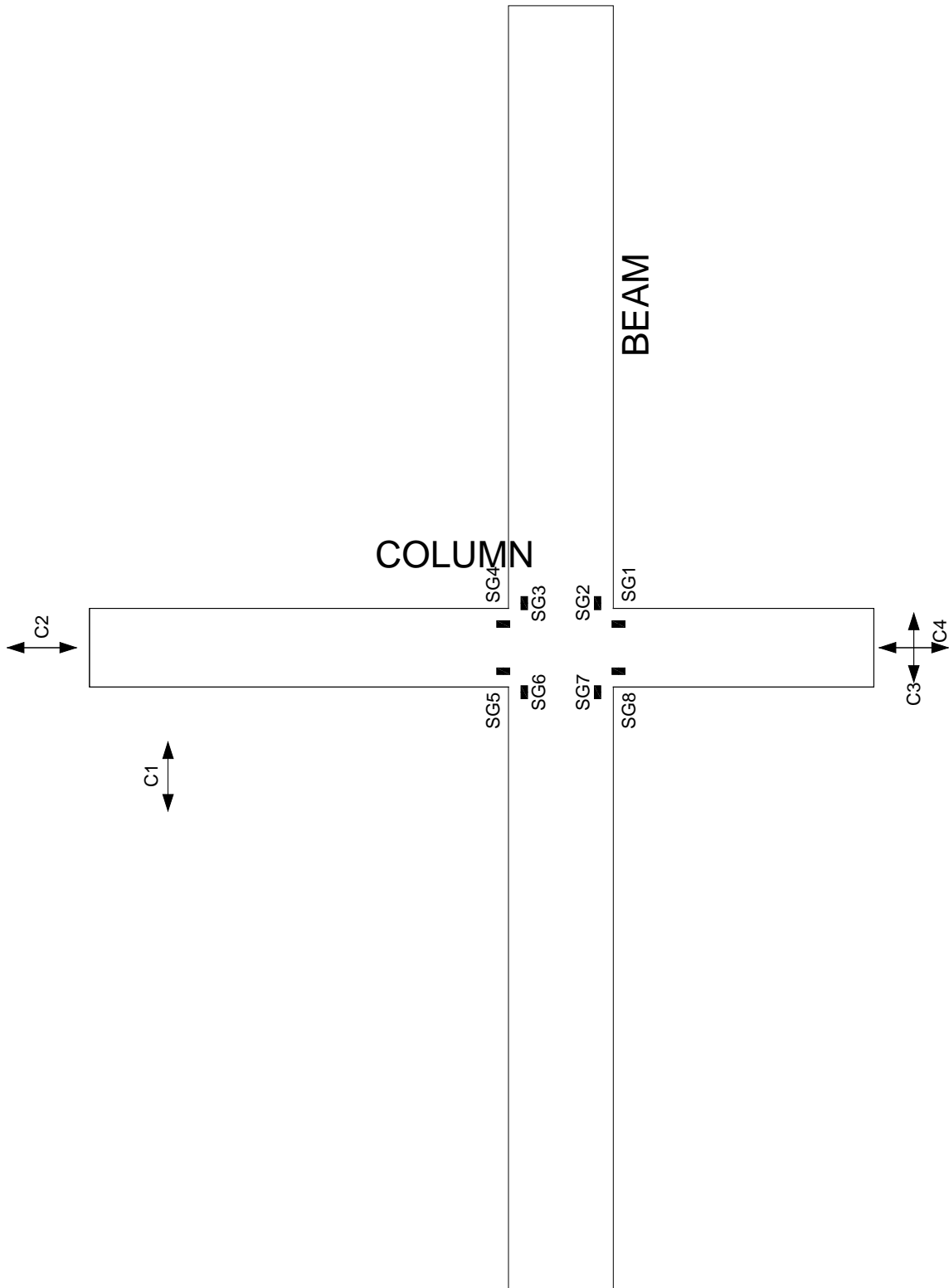
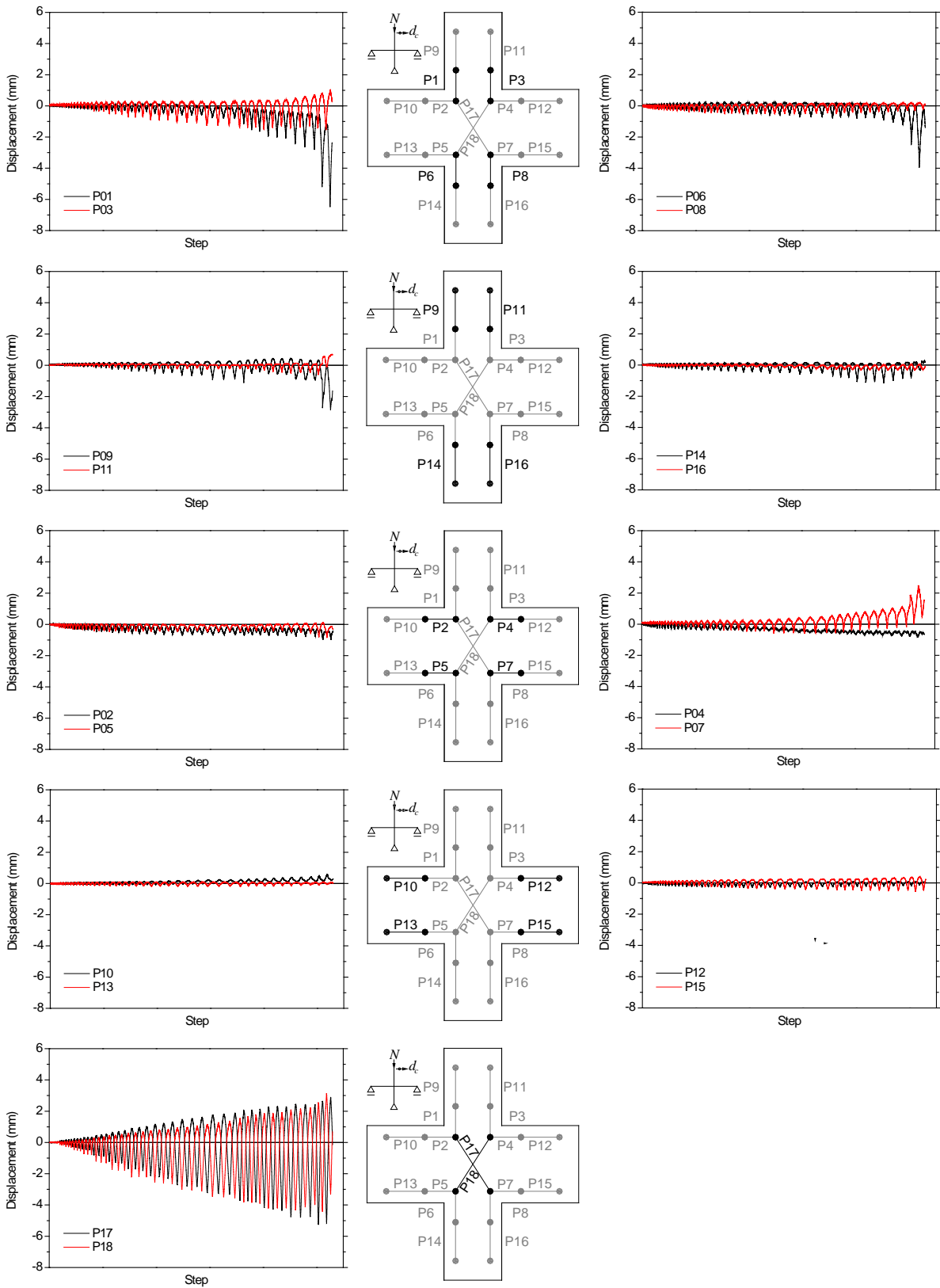


Figure I.2 – Location of the strain gauges.

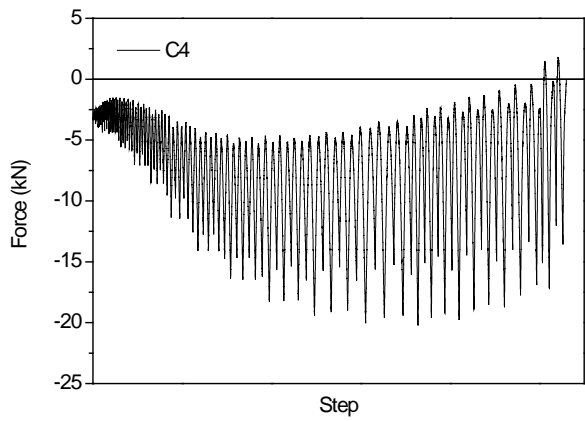
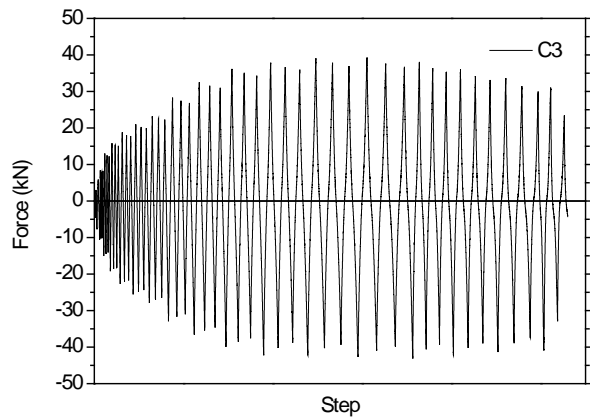
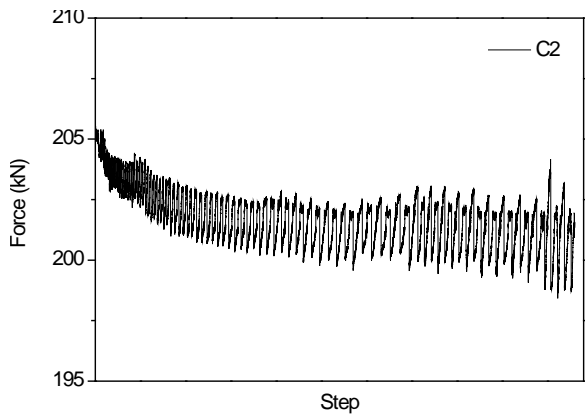
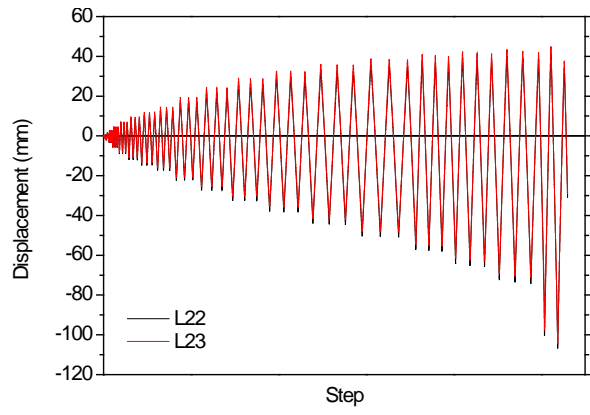
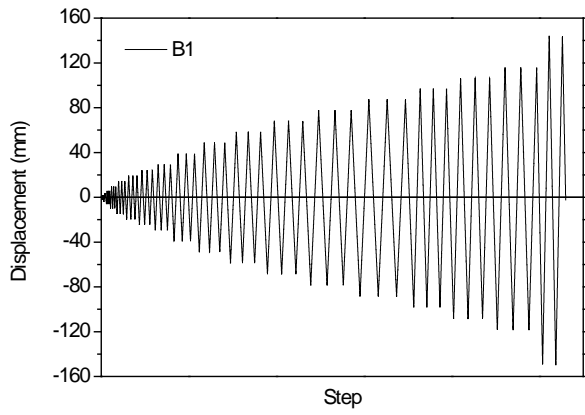
## **ANNEX II**

---

**RESULTS OF SPECIMEN JDR**



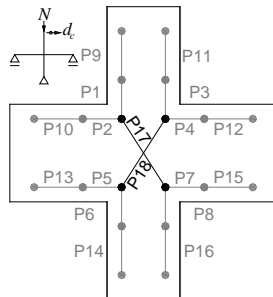
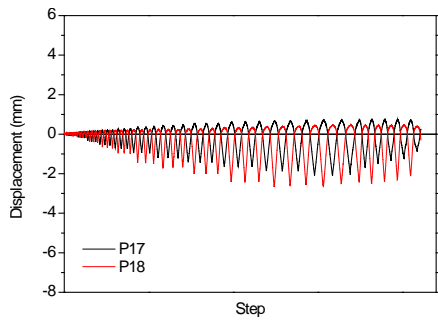
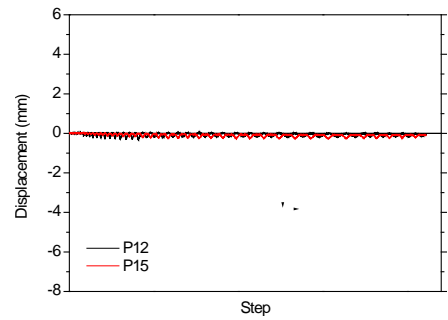
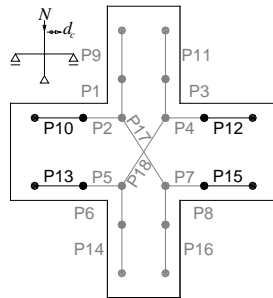
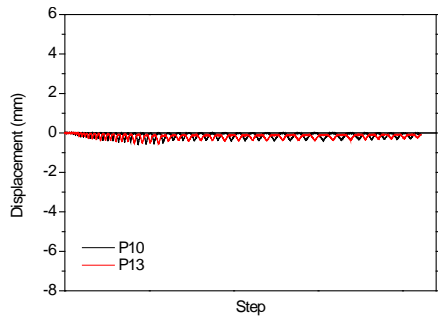
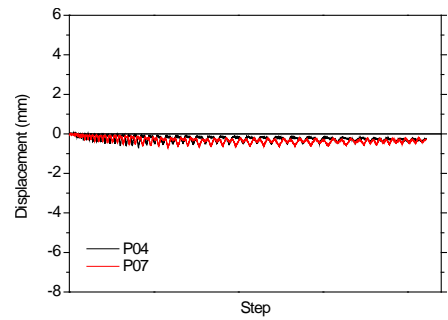
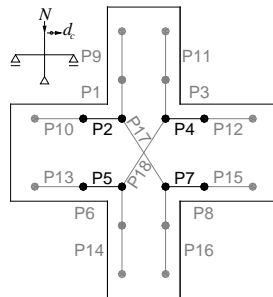
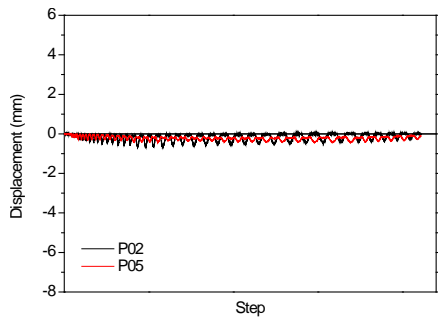
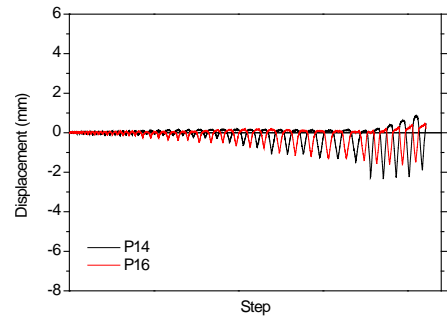
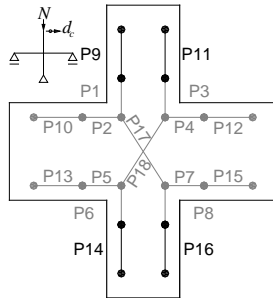
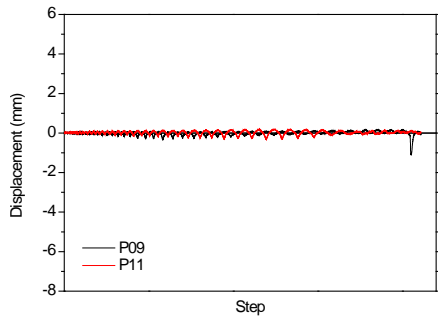
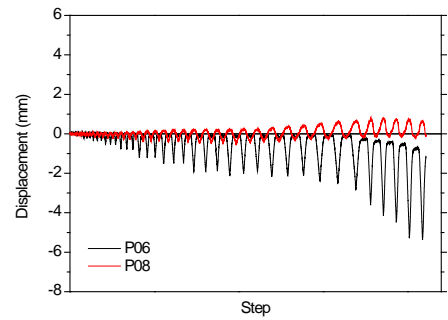
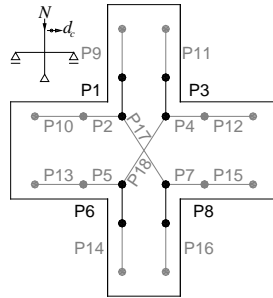
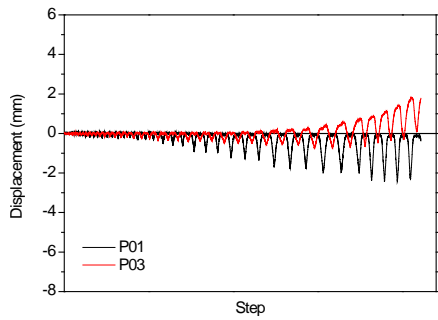


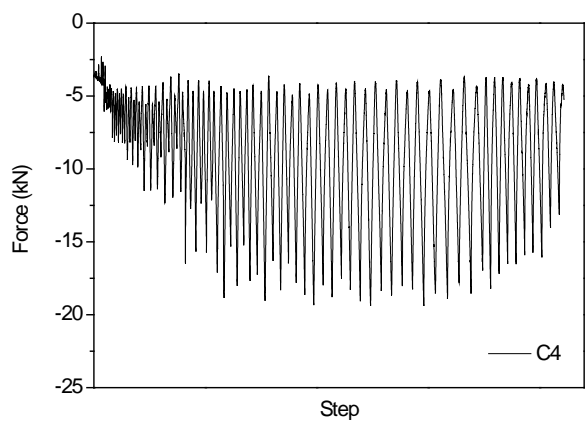
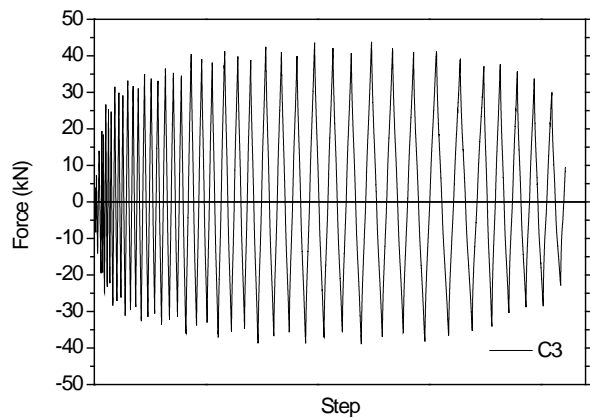
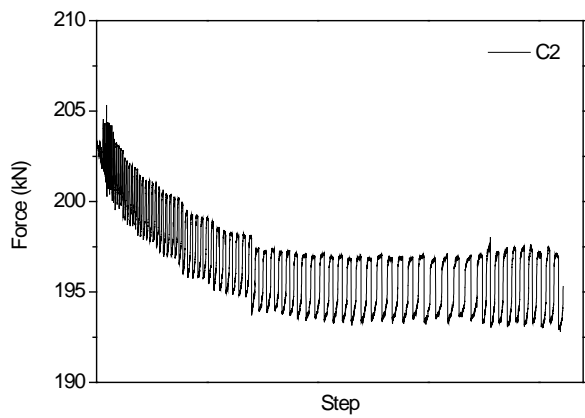
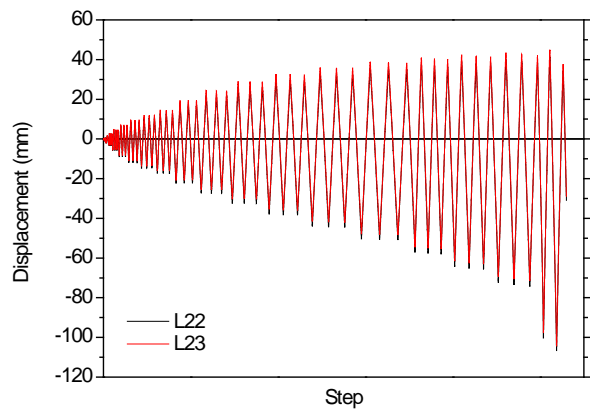
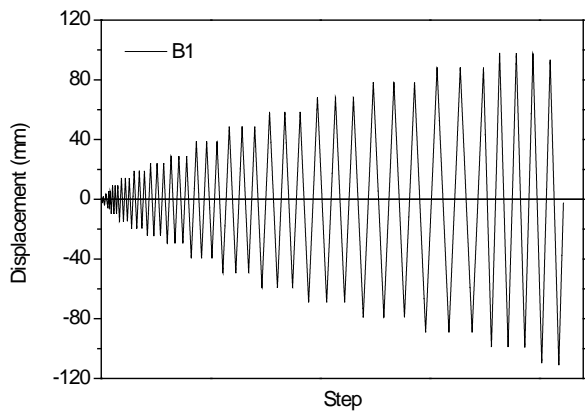


# **ANNEX III**

---

**RESULTS OF SPECIMEN JPA-1R**





# **ANNEX IV**

---

**RESULTS OF SPECIMEN JPA-2R**

